Physics of the Earth and Planetary Interiors 171 (2008) 336–356

Contents lists available at ScienceDirect

Physics of the Earth and Planetary Interiors

journal homepage: www.elsevier.com/locate/pepi

Numerical modelling of crustal growth in intraoceanic volcanic arcs

Ksenia Nikolaeva*, Taras V. Gerya, James A.D. Connolly

Department of Geosciences, Swiss Federal Institute of Technology (ETH-Zürich), CH-8092 Zurich, Switzerland

ARTICLE INFO

Article history:
Received 29 October 2007
Received in revised form 7 May 2008
Accepted 30 June 2008

Keywords:
Numerical modelling
Intraoceanic subduction
Magmatic addition
Crustal growth rate

ABSTRACT

We investigate crustal growth processes on the basis of a 2D coupled geochemical–petrological–thermomechanical numerical model of retreating intraoceanic subduction. The model includes spontaneous slab retreat and bending, subducted crust dehydration, aqueous fluid transport, mantle wedge melting, and melt extraction resulting in crustal growth. Our numerical experiments show that the rate of plate retreat influences both the rate of crust formation and composition of newly formed crust. The rate of trench retreat, which is a manifestation of subduction rate, strongly varies with time: retreat rates slow (from 7 cm/a to 1 cm/a) shortly (in a few Ma) after the beginning of subduction and then increase (up to 4 cm/a). Subsequently two different scenarios can be distinguished: (1) subduction rate decay that leads ultimately to cessation of subduction, (2) subduction rate acceleration (up to 12 cm/a), which stabilizes subduction. The rate of crust formation positively correlates with rate of trench retreat. Modelled average rates of crustal growth (30–50 km^3/km/Ma) do not include effects of dry mantle melting and are close to the lower edge of the observed range of rates for real arcs (40–180 km^3/(km Ma)). The composition of new crust depends strongly on the evolution of subduction. Four major magmatic sources can contribute to the formation of the crust: (1) hydrated partially molten peridotite of the mantle wedge, (2) melted subducted sediments, (3) melted subducted basalts, (4) melted subducted gabbro. Crust produced from the first source is always predominant. In all studied cases it appears shortly after beginning of subduction and is a persistent component so long as subduction remains active. Significant amount of crust produced from other three sources appear (i) in the beginning of subduction due to the melting of the slab "nose" and (ii) at later stages when subduction velocity is low (<1 cm/a), which leads to the thermal relaxation of the slab. Both the intensity of melt extraction, which was prescribed by given melt extraction threshold, and the age of subducted plate affect the volume of new crust. On a long time scale the greatest volume of magmatic arc crust is formed with an intermediate melt extraction threshold (2–6%) and medium subducted plate ages (70–100 Ma).

1. Introduction

Subduction zones integrate the Earth's crust with the mantle. This integration occurs by the sinking of oceanic crust into the mantle and the formation of new crust by fluids and melt released from the slab and suprajacent mantle. We concentrate here on the crustal growth aspect of subduction zones. The deformation and metamorphism of crust, contamination and mixing of initial magmas, lack of data, and complex geological setting and geodynamics history make investigation by natural observations difficult. Yet progress in this topic has been made through geochemistry. Isotopic and trace element ratios have established magmatic sources (e.g. Tera et al., 1986; Elburg et al., 2004; Kessel et al., 2005; Saal et al., 2005) and the mode of mass transport (e.g. Hawkesworth et al., 1997; George et al., 2003; Elliott et al., 1997). The role of slab derived melts is debated because subducted oceanic crust in most modern subduction zones is thought to be too cold to permit slab melting (Schmidt and Poli, 1998; Peacock et al., 1994). Nevertheless, a slab component is necessary to explain geochemical features of arc lavas, e.g. high LILE/HFSE and LREE/HFSE ratios as compared to the ratios typical of mantle-derived melts in other tectonic settings (Macpherson et al., 2006; Armstrong, 1971; Tera et al., 1986; Rosner et al., 2003). Accordingly, some authors explain these features as a consequence of slab melting (Kelemen et al., 1990, 2003), while other authors invoke transport by hydrous fluids released from the slab (Tatsumi et al., 1986). More recently we have argued that crustal component can also be explained by hydrated partially molten diapiric upwellings (cold plumes) rising from slabs (Gerya and Yuen, 2003b; Gerya et al., 2006). Another controversial problem in the crustal production process within subduction zone is the relation of geodynamics to the composition of arc rocks. To some extent, this problem has been resolved by geochemistry

* Corresponding author.
E-mail address: nikolaeva@erdw.ethz.ch (K. Nikolaeva).

0031-9201/$ – see front matter © 2008 Elsevier B.V. All rights reserved.
doi:10.1016/j.pepi.2008.06.026

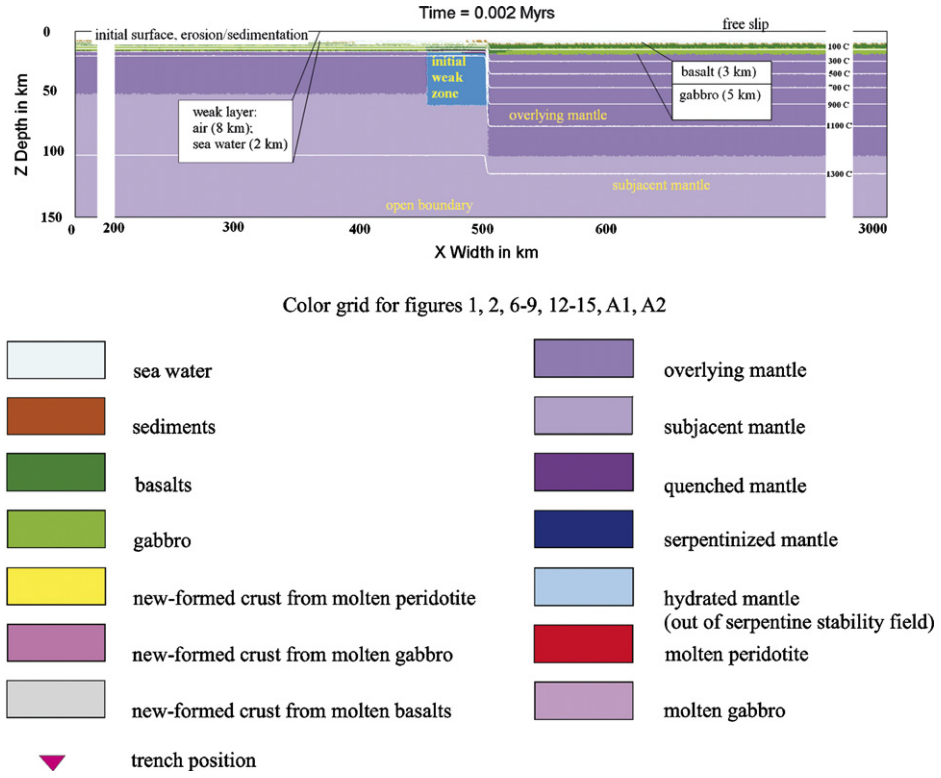

Fig. 1. Initial configuration of numerical model (see text for details). Staggered grid resolution: 651 × 101 nodes, 10 million randomly distributed markers. Grid step varies from 2 km × 2 km in the subduction zone area to 10 km × 2 km outside of this area.

Table 1
Model rock compositions (wt.%)

	Sediment	Upper oceanic crust (altered basalt)	Lower oceanic crust (gabbro)	Mantle (peridotite)
SiO_2	61.10	47.62	53.49	45.55
Al_2O_3	12.43	14.48	14.07	4.03
FeO	5.43	10.41	6.86	7.47
MgO	2.59	6.92	12.07	37.42
CaO	6.21	13.39	10.73	3.18
Na_2O	2.54	2.15	1.22	0.33
K_2O	2.13	0.58	0.09	0.03
H_2O	7.60	2.78	1.47	1.98

Sediment is the GLOSS average (Plank and Langmuir, 1998); basalt is an average for the upper 500 m of the igneous section of the oceanic crust (Staudigel et al., 1989); gabbro is a synthetic composition for the gabbroic section of the oceanic crust (Behn and Kelemen, 2003), modified to contain up to 1.5 wt.% water to represent the effects of lower crustal hydrothermal alteration (Carlson, 2001), and peridotite is the LOSIMAG composition (Morris and Hart, 1986) chosen to represent mantle peridotite. The compositions have been simplified by the omission of minor elements such as Mn, P, Ti, and Cr and the assumption that all Fe is ferrous; additionally CO_2 has been removed from the GLOSS sediment composition.

Table 2
Material properties used in numerical experiments

Material	Thermal conductivity ($Wm^{-1}\,K^{-1}$)	Rheology	$T_{solidus}$ (K)	$T_{liquidus}$ (K)
Sedimentary rocks	$0.64+\frac{807}{T+77}$	Wet quartzite flow law, c = 3–10 MPa, $\sin(\varphi)=0$	$889+17900/(P+54)+20200/(P+54)^2$ at $P<1200$ MPa, $831+0.06P$ at $P>1200$ MPa	$1262+0.09P$
Upper oceanic crust (altered basalt)	$1.18+\frac{474}{T+77}$	Wet quartzite flow law, c = 3–10 MPa, $\sin(\varphi)=0$	$973-70400/(P+354)+77800000/(P+354)^2$ at $P<1600$ MPa, $935+0.0035P+0.0000062P^2$ at $P>1600$ MPa	$1423+0.105P$
Lower oceanic crust (gabbro)	–//–	Plagioclase (An_{75}) flow law, c = 3 MPa, $\sin(\varphi)=0.15$	–//–	–//–
Serpentinized mantle	$0.73+\frac{1293}{T+77}$	Wet olivine flow law, c = 3 MPa, $\sin(\varphi)=0$, constant viscosity = 10^{18}–10^{19} Pa s	–	–
Hydrated unserpentinized mantle	–//–	Wet olivine flow law, c = 3 MPa, $\sin(\varphi)=0$	$1240+49800/(P+323)$ at $P<2400$ MPa, $1266-0.0118P+0.0000035P^2$ at $P>2400$ MPa	$2073+0.114P$
Dry mantle	–//–	Dry olivine flow law, c = 1 MPa, $\sin(\varphi)=0.6$	–	–
References	Clauser and Huenges (1995)	Rannalli (1995)	Schmidt and Poli (1998), Poli and Schmidt (2002)	Schmidt and Poli (1998), Poli and Schmidt (2002)

Table 3
Phases and thermodynamic data sources

Phase	Formula	Source
Antigorite	$Mg_{48x}Fe_{48(1-x)}Si_{34}O_{85}(OH)_{62}$	Rupke et al. (2004)
Clinoamphibole	$Ca_{2-2w}Na_{z+2w}Mg_{(3+2y+z)x}Fe_{(3+2y+z)(1-x)}Al_{3-y-w}Si_{7+w+y}O_{22}(OH)_2$ $w+y+z\leq 1$	Wei and Powell (2003), White et al. (2003)
Biotite	$KMg_{(3-w)x}Fe_{(3-w)(1-x)}Al_{1+2w}Si_{3w}O_{10}(OH)_2$ $x+y\leq 1$	Powell and Holland (1999)
Chlorite	$Mg_{(5-y+z)x}Fe_{(5-y+z)(1-x)}Al_{2(1+y-z)}Si_{3-y+z}O_{10}(OH)_8$	Holland et al. (1998)
Coesite	SiO_2	
Clinopyroxene	$Na_{1-y}Ca_yMg_{xy}Fe_{(1-x)y}Al_ySi_2O_6$	Holland and Powell (1996)
Fluid	H_2O	Holland and Powell (1998)
Garnet	$Fe_{3x}Ca_{3y}Mg_{3(1-x-y)}Al_2Si_3O_{12}$, $x+y\leq 1$	Holland and Powell (1998)
Kyanite	Al_2SiO_5	
Lawsonite	$CaAl_2Si_2O_7(OH)_2\cdot H_2O$	
Mica	$K_xNa_{1-x}Mg_yFe_zAl_{3-2(y+z)}Si_{3+y+z}O_{10}(OH)_2$	Holland and Powell (1998)
Melt	Na–Mg–Al–Si–K–Ca–Fe hydrous silicate melt	Ghiorso et al. (2002)
Olivine	$Mg_{2x}Fe_{2(1-x)}SiO_4$	Holland and Powell (1998)
Ortopyroxene	$Mg_{x(2-y)}Fe_{(1-x)(2-y)}Al_{2y}Si_{2-y}O_6$	Holland and Powell (1996)
Plagioclase	$Na_xCa_{1-x}Al_{2-x}Si_{2+x}O_8$	Newton et al. (1980)
Sanidine	$Na_xK_{1-x}AlSi_3O_8$	Thompson and Hovis (1979)
Stishovite	SiO_2	
Talc	$Mg_{(3-y)x}Fe_{(3-y)(1-x)}Al_{2y}Si_{4-y}O_{10}(OH)_2$	Holland and Powell (1998)

(e.g. Gordienko et al., 2007; Encarnacion, 2004). Straub (2003) used major element chemistry to explain the transition from boninitic to tholeiitic volcanism in Izu Bonin–Mariana system by large scale replacement of mantle wedge material. Stern et al. (2006) speculate that geochemical and isotopic variations of Guguan cross-chain basalts are result of an increasing role of fluids released from serpentinites interacting with relatively enriched OIB-type mantle.

Various aspects of subduction zone processes related to volcanic arc growth have been studied numerically, e.g. initiation of subduction (Regenauer-Lieb et al., 2001; Hall et al., 2003); water release and its influence on subduction dynamics (Iwamori, 1998; Gerya et al., 2002; Rupke et al., 2004); slab melting (e.g. Peacock et al., 1994; Gerya and Yuen, 2003b; Gerya et al., 2004a); seismic features related to mantle wedge melting (Gerya et al., 2006; Gorczyk et al., 2006); and sub-arc magmatic productivity (Gorczyk et al., 2007a,b). However the dynamics of crustal growth in 2D has not been modelled numerically. In this paper we study this process with a 2D coupled geochemical–petrological–thermomechanical numerical model of retreating intraoceanic subduction. The model includes spontaneous slab retreat and bending, subducted crust dehydration, aqueous fluid transport, mantle wedge melting, and melts extraction resulting in crustal growth.

2. Model description

2.1. Initial and boundary conditions

Our 2D model (Fig. 1, Table 1) simulates initiation and development of intraoceanic subduction resulting in volcanic arc growth in a 3000 km × 200 km lithospheric/upper mantle section. The oceanic crust is represented by a 2-km thick upper layer of hydrothermally altered basalts overlying 5 km of gabbroic rocks, and the mantle consists of anhydrous peridotite. The model oceanic crust does not include sediments, but sediments spontaneously fill the trench after its arc-ward slope reaches certain critical steepness. In addition to the water bound in hydrous minerals, 2 wt.% connate water is initially present in the basaltic and sedimentary sections of the subducted oceanic crust.

In the model, subduction is initiated by a prescribed weak fracture zone between two oceanic plates of different ages (Hall et al., 2003). This zone is 30 km wide and 60 km thick. It consists of mantle rocks with wet olivine rheology (Rannalli, 1995) and high pore fluid pressure. In the course of subduction, these mantle rocks are replaced by weak crustal rocks and hydrated mantle thereby naturally preserving the localizing effect of the initially prescribed fracture zone. Recent dynamic models of subduction process, with visco-(elasto)-plastic rheology (Hassani et al., 1997; Hall et al., 2003; Sobolev and Babeyko, 2005; Tagawa et al., 2007; Gorczyk et al., 2007b; Gerya et al., 2008) have shown that stable one-sided

Table 4
Description of numerical experiments

Model	Slab age (Ma)	Melt extraction threshold (vol.%)	v_{fl}[a] (m/a)
1	40	0.2	0.09
2	40	0.4	0.09
3	40	1	0.09
4	40	2	0.09
5	40	4	0.09
5′1	40	4	0.009
5′2	40	4	0.0009
6	40	6	0.09
7	40	10	0.09
8	40	14	0.09
9	40	18	0.09
10	40	30	0.09
11	70	0.2	0.09
12	70	0.4	0.09
13	70	1	0.09
14	70	2	0.09
15	70	4	0.09
15′1	70	4	0.009
15′2	70	4	0.0009
16	70	6	0.09
17	70	10	0.09
18	70	14	0.09
19	70	18	0.09
20	70	30	0.09
21	100	0.2	0.09
22	100	0.4	0.09
23	100	1	0.09
24	100	2	0.09
25	100	4	0.09
25′1	100	4	0.009
25′2	100	4	0.0009
26	100	6	0.09
27	100	10	0.09
28	100	14	0.09
29	100	18	0.09
30	100	30	0.09

[a] v_{fl} is the constant velocity of upward percolation of water through the mantle.

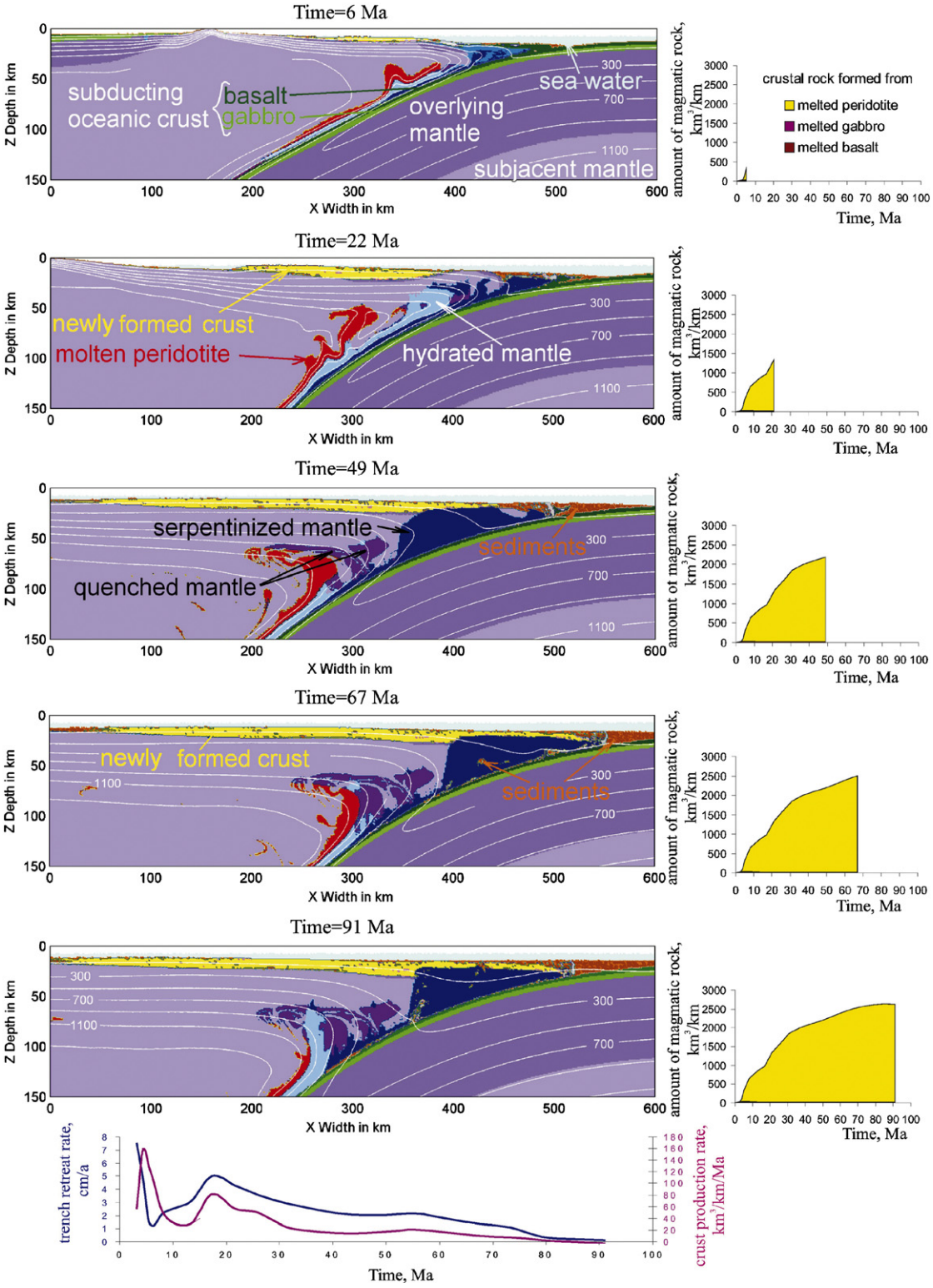

Fig. 2. Common evolution of temperature and lithological fields in our experiments (model 24, Table 4). Color grid is as on the Fig. 1. Changing of rate of plate retreat and crust accumulation rate with time for this experiment is depicted below. Time is dated from the beginning of subduction. Subduction results in a hydration and partial melting of mantle wedge rocks, which leads to the formation of volcanic arc straightly over the area of melting. The melt propagation up to the surface was not modelled here. It can be related to the formation of magmatic channels (Gerya and Burg, 2007) and its rate is assumed to be much higher that the rate of mantle rocks deformation (Elliott et al., 1997; Hawkesworth et al., 1997).

subduction requires a low strength interface between strong plates. These studies indicate that effective friction coefficient at subduction interface must be below 0.1 to enable stable subduction. As such friction coefficients are lower than experimental values for dry solid rocks the low strength interface has been attributed to presence of metamorphic fluids (e.g. Hall et al., 2003; Gerya et al., 2008). Following arguments of Gerya et al. (2008) we assumed that pressure of free porous fluid in dehydrating subducted crust and hydrated mantle formed along the slab will be close to mean stress on solid phases and respectively lowered internal friction angle φ for these rocks to 0 (Table 2).

In the evolution of the model water is expelled from the subducted oceanic crust as a consequence of dehydration reactions and compaction. To account for the release of connate water by compaction, the connate water content of the basaltic and sedimentary crust is specified as a linear function of depth.

$$X_{H_2O(p)}(\text{wt.\%}) = X_{H_2O(p0)}(1 - 0.02\Delta z), \quad (1)$$

where $X_{H_2O(p0)} = 2$ wt.% is the connate water content at the surface, Δz (km) is depth below the surface in km (0–50 km). The timing of water release by dehydration reactions is determined by the model physicochemical conditions and the assumption of thermodynamic equilibrium. Water transport velocity is computed as (Gorczyk et al., 2007b):

$$v_{x(\text{water})} = v_x, \qquad v_{z(\text{water})} = v_z - v_{z(\text{percolation})}, \quad (2)$$

where v_x and v_z are local velocity of the mantle and $v_{z(\text{percolation})}$ is the prescribed relative velocity of upward percolation of water through the mantle (0.001, 0.009, 0.09 m/y in our experiments).

The water expelled from the slab migrates upward until it reaches mantle rocks, which can consume an additional amount of water by hydration reactions. We assume incomplete hydration of the mantle wedge as a consequence of the channelization of slab-derived fluids (Davies, 1999). To account for this behavior, we arbitrarily assign 2 wt.% water as an upper limit for mantle wedge hydration. For comparison, Carlson and Miller (2003) argue on the

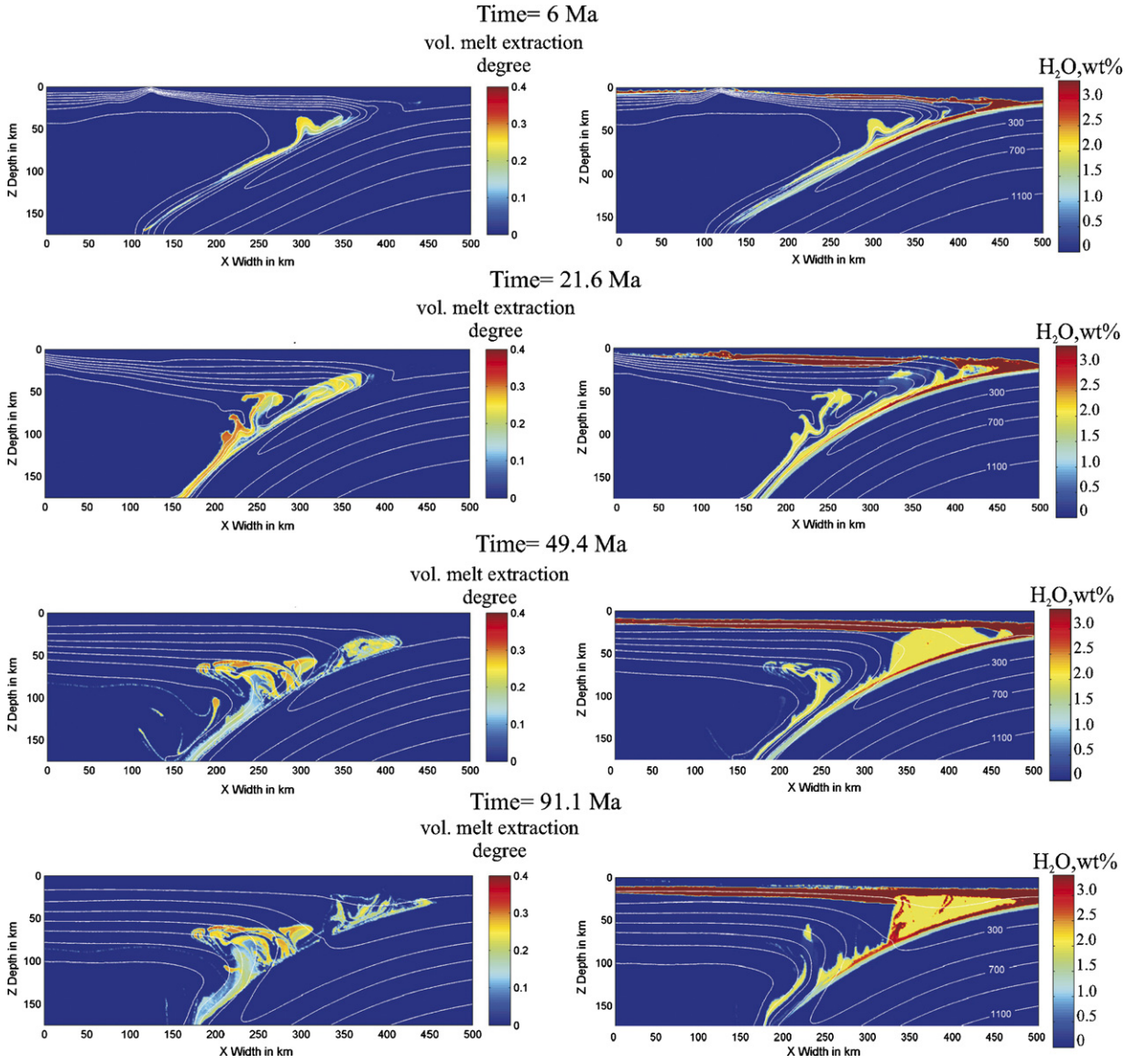

Fig. 3. Evolution of degree of melt extraction (left column) and water content (right column) in the mantle wedge and subducting oceanic crust. Corresponding lithological field is depicted on the Fig. 2.

basis of seismic data that few mantle wedges achieve average water contents above ~4 wt.% and true water saturation is predicted at ~8 wt.% (Connolly, 2005). The hydrated mantle is subdivided into two parts: an upper, serpentinized, subduction channel, and a lower, hydrated, but not serpentinized zone. The stable hydrous phases in peridotite were calculated (see petrological part of model design) for each P–T conditions and equilibrium water content (≤2 wt.%).

Because the water transport model does not permit complete hydration of the peridotitic mantle, the mantle solidus is intermediate between the wet and dry peridotite solidi. In reality variable hydration would permit melting over a range of temperatures and water contents (e.g. Grove et al., 2006). To account for this behavior we assume, as in our previous papers (e.g. Gerya and Yuen, 2003a), that the degree of hydrous melting is a linear function of pressure and temperature. In this model the volumetric degree of melting M_0 is (Gerya and Yuen, 2003a):

$$M_0 = \begin{cases} 0 & T < T_{\text{solidus}} \\ \dfrac{T - T_{\text{solidus}}}{T_{\text{liquidus}} - T_{\text{solidus}}} & T_{\text{solidus}} < T < T_{\text{liquidus}} \\ 1 & T > T_{\text{liquidus}} \end{cases} \quad (3)$$

where T_{solidus} and T_{liquidus} are, respectively, wet solidus temperature and dry liquidus temperature at a given pressure and rock composition (Table 2). To simulate melt extraction from partially molten rocks we define melt extraction threshold $M_{\max}$ and non-extractable amount of melt $M_{\min} < M_{\max}$ remaining in the rock. The influence of these parameters on subduction dynamics and crustal growth is investigated for the case of constant $M_{\max}/M_{\min} = 2$ ratio.

The amount of melt extracted during the model evolution is tracked by markers. Total amount of melt M for every marker takes into account amount of previously extracted melt and is calculated as

$$M = M_0 - \sum_n M_{\text{ext}}, \quad (4)$$

where $\sum_n M_{\text{ext}}$ is the total melt fraction extracted during the previous n extraction episodes. Once the total amount of melt M computed from Eqs. (3) and (4) for given marker exceeds $M_{\max}$, the extractable melt fraction $M_{\text{ext}} = M - M_{\min}$ is assumed to migrate upward and the value of $\sum_n M_{\text{ext}}$ is updated. We assume that melt migration is rapid compared to the deformation of unmelted mantle, so that the velocity of the melt is independent of mantle dynamics (Elliott et al., 1997; Hawkesworth et al., 1997). Thus, the extracted melt is transported instantaneously to the surface forming volcanic arc crust.

All mechanical boundary conditions are free-slip, except the lower boundary, which is permeable in vertical direction (Gorczyk et al., 2007b). The top surface of oceanic crust made to be essentially an internal free surface by using a 10-km thick top layer with low

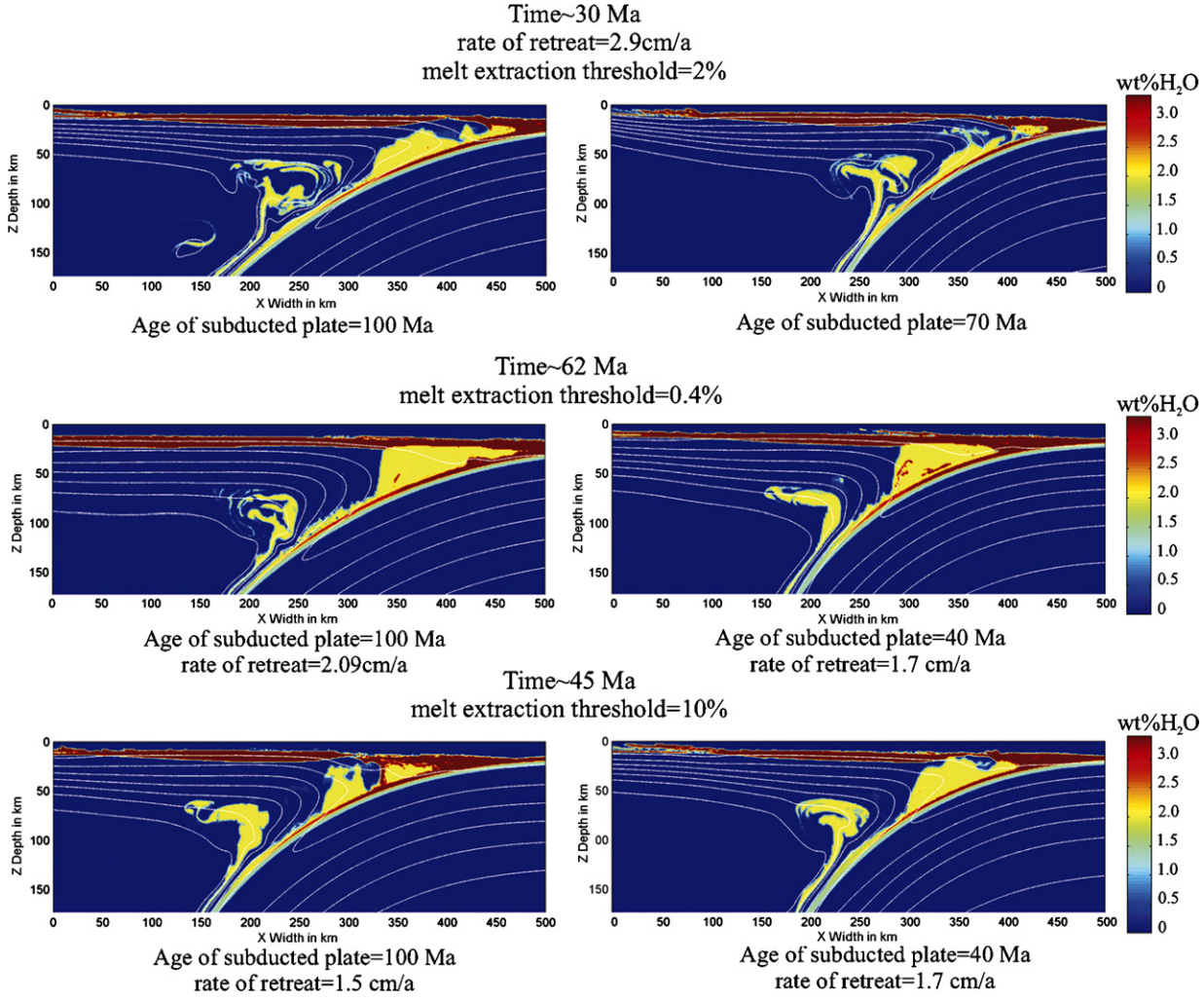

Fig. 4. Water content in the mantle wedge as a function of age of subducting plate (models from top to the bottom: 24 versus 14, 22 versus 2, and 27 versus 7).

viscosity (10^{19} Pa s) and density (1 kg/m^3 for the air, 1000 kg/m^3 for the water). The large viscosity contrasts caused by these low viscosity boundary layers minimize shear stresses (<10^4 Pa) at the top of the solid portion of the model. This upper boundary evolves by erosion and sedimentation as dictated by the transport equation:

$$\frac{\partial z_{es}}{\partial t} = v_z - v_x \frac{\partial z_{es}}{\partial x} - v_s + v_e, \quad (5)$$

where z_{es} is a vertical position of the surface as a function of the horizontal distance x; v_z and v_x are vertical and horizontal components of material velocity vector at the surface; v_s and v_e are sedimentation and erosion rates, respectively, which correspond to relations:

$$v_s = 0\,\text{mm/y}, \quad v_e = v_{e0}\,\text{mm/y}, \quad \text{when } z < 8\,\text{km},$$
$$v_s = v_{s0}\,\text{mm/y}, \quad v_e = 0\,\text{mm/y}, \quad \text{when } z > 8\,\text{km},$$

where $v_{e0} = 0.3$ mm/y and $v_{s0} = 0.03$ mm/y are imposed erosion and sedimentation rates, respectively; $z = 8$ km is the sea-level prescribed in the model. We used low gross scale sedimentation rates in our models to preclude global growth of sedimentary layer on the surface of the oceanic plate. A sedimentary layer is added at the trench when its arc-ward slope exceeds a critical angle of 17°.

The subducted plate is attached to the right boundary, thus subduction is manifest by the retreat of subducted plate. This behavior does not significantly affect dynamics of subduction and crustal growth in our models (Appendix A).

The initial temperature field for oceanic plates is an oceanic geotherm (Turcotte and Schubert, 2002) for different lithosperic ages (40, 70, 100 Ma for subducted plates and 1 Ma for young overlying oceanic plate).

2.2. Petrological model

The stable mineralogy for each lithology as a function of pressure and temperature was computed from thermodynamic data (Table 3, for details see Gerya et al., 2006) by free energy minimization (Connolly, 2005; Connolly and Petrini, 2002). Seismic velocities were calculated as outlined by Connolly and Kerrick (2002), with shear moduli as summarized in (Connolly, 2005). We computed bulk velocities from volumetrically weighted arithmetic mean of the relevant elastic moduli for the stable phases. The bulk velocities include the silicate melt but do not include free water, the amount of which is assumed to be negligible (Gerya et al., 2006).

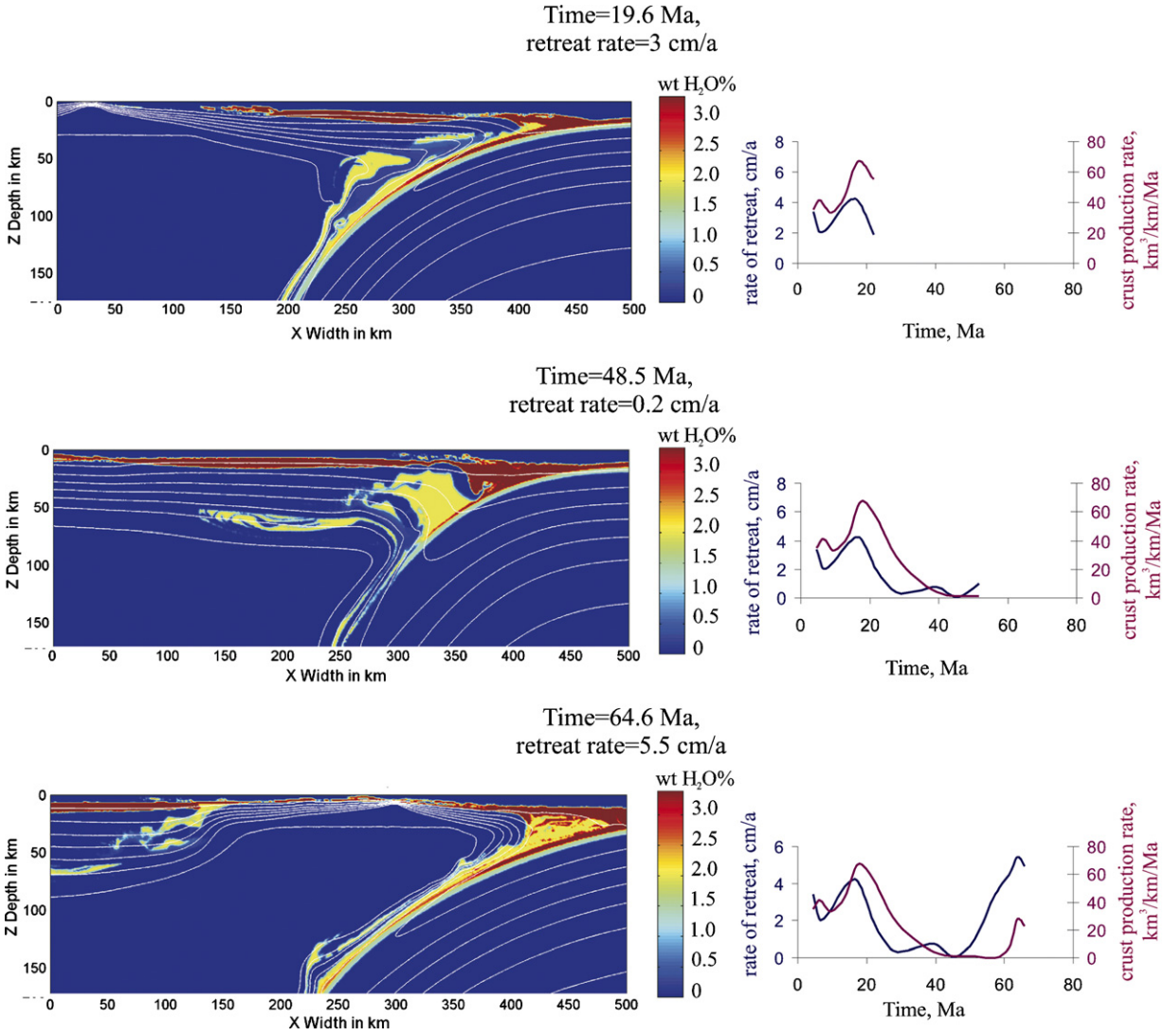

Fig. 5. Water content in the mantle wedge as a function of rate of plate retreat (model 6, Table 4).

2.3. Numerical implementation

Our model is based on the I2VIS code (Gerya and Yuen, 2003b), which combines a conservative finite difference method with a non-diffusive-marker-in-cell technique. To account for thermal and density effects of phase transformations we employ the incompressible fluid approximation for the continuity equation and numerical smoothing of thermal and density effects due to phase changes for the momentum and temperature equations (Gerya et al., 2006).

3. Results

3.1. General development

To investigate the dynamics of arc growth and displacement we carried out three series of numerical experiments systematically varying the age of the subducting plate (40, 70 and 100 Ma) and the efficiency of melt extraction (melt extraction threshold M_{max} values from 0.2 to 30 vol.%). Another series of experiments was conducted to investigate the influence of the velocity of fluid migration (Table 4).

As a consequence of increasing of pressure and temperature during subduction the subducted oceanic crust releases water (Figs. 2 and 3). At the onset of subduction this water release is primarily the result of the expulsion of connate water (Iwamori, 1998). At greater depths, water is released at somewhat lower rates by metamorphic dehydration. The upper oceanic crust releases most of its water at depth <100 km, while the lower oceanic crust dehydrates at greater depths releasing water at lower rates (Rupke et al., 2004); and it can retain water up to 150–200 km depths (Schmidt and Poli, 1998). The intensity of metamorphic dehydration depends on hydrous phase stability and hence on the slab geotherm. As slab temperature varies inversely with slab age and subduction rate, dehydration occurs at shallower depth for younger slabs (Fig. 4) (Iwamori, 1998) and slower subduction (Fig. 5); as also reported by Rupke et al. (2004). Other factors may also influence the magnitude and dynamics of water release, e.g. duration of subduction (defining thermal structure of the overriding plate) and slab dip (e.g. Gorczyk et al., 2007b).

Water released into the mantle wedge may hydrate the mantle rocks to form a serpentinized layer above the slab to a depth of 100–130 km (Fig. 2). At greater depths, the water may induce melting (e.g. Davies and Stevenson, 1992; Stern, 2002; Takahashi and Kushiro, 1983). Both processes generate Rayleigh–Taylor instabilities along the slab (Gerya and Yuen, 2003b) and induce "cold plume" upwellings (Fig. 2). The intensity of these upwellings depends on factors such as rate of trench retreat, subducting plate age, and melt extraction threshold M_{max}. The quantity and com-

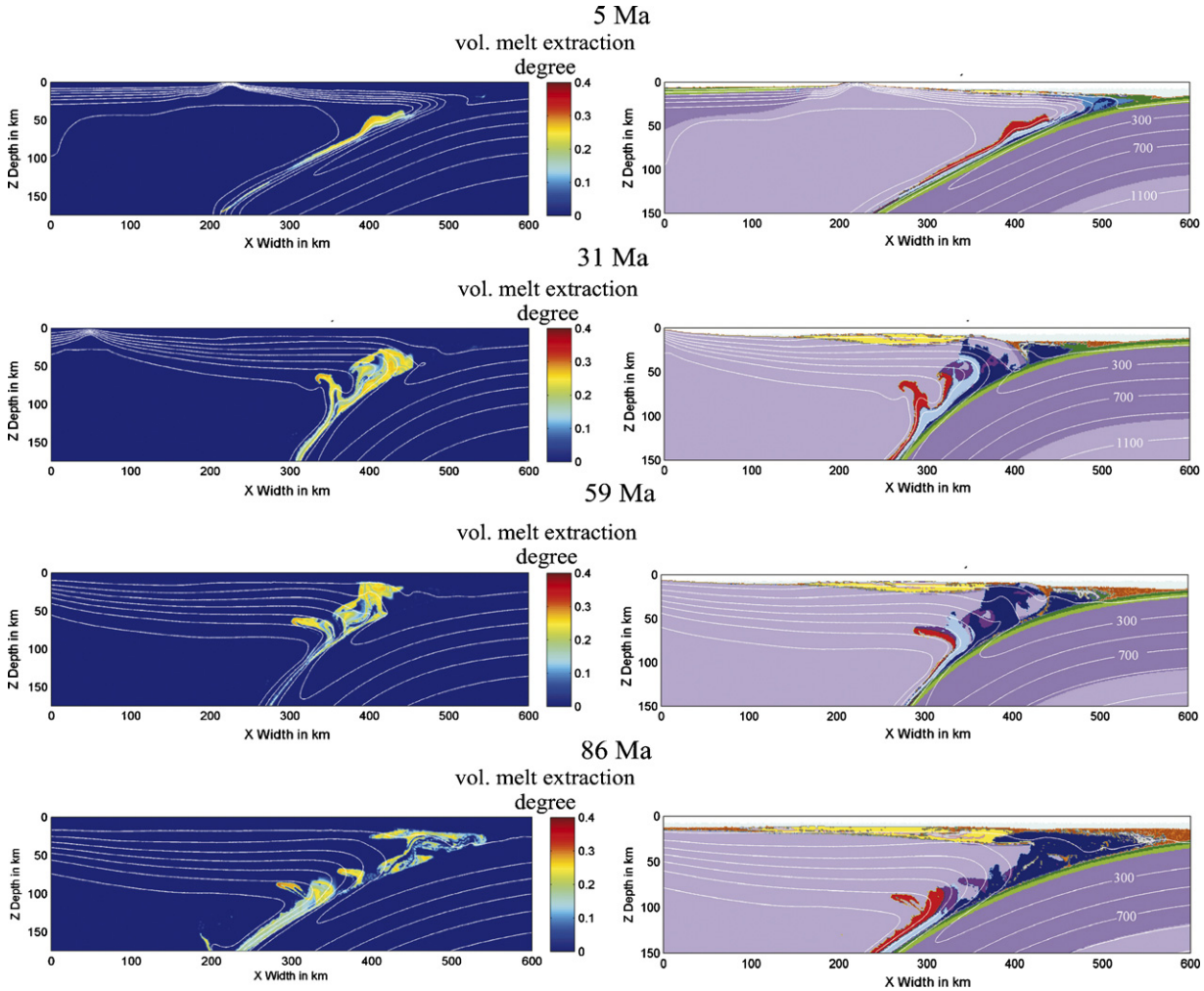

Fig. 6. Model 21, Table 4: degree of melt extraction (mantle depletion) in the mantle wedge (left column) and corresponding composition and temperature fields (right column, color code is the same as in Fig. 1). The residue of partially molten peridotite can be re-hydrated by new portions of slab released fluids and then either contributes to hydrated (serpentinized) mantle or takes part in the next melting event. In the first case it may reach the surface within the serpentinized channel (time = 59 and 86 Ma).

position of these plumes strongly influences the dynamics of melt extraction and crustal development.

Melting and melt extraction occur as long as there is fluid release from the subducted plate. Thus, some parts of the mantle wedge undergo multiple melting events and become depleted. In the Figs. 3 and 6 mantle wedge depletion is characterized in terms of degree of melt extraction. This depleted mantle material may become entrained in plumes and reach the surface as xenoliths in arc lavas (e.g. Nimz et al., 1995). Alternatively, it may be re-hydrated and then contribute to generation of the new melts or remains in the colder portions of the wedge as hydrated (serpentinized) mantle. In the first case one should find a signature of a more depleted mantle component in the arc lavas (e.g. Melcher et al., 2002). In the second case cold re-hydrated depleted mantle can be involved into the circulation within serpentinized subduction channel where it become mixed with other types of rocks (Fig. 6) including subducted oceanic crust, non-depleted serpentinized lithospheric mantle of the overriding plate and serpentinites derived from the

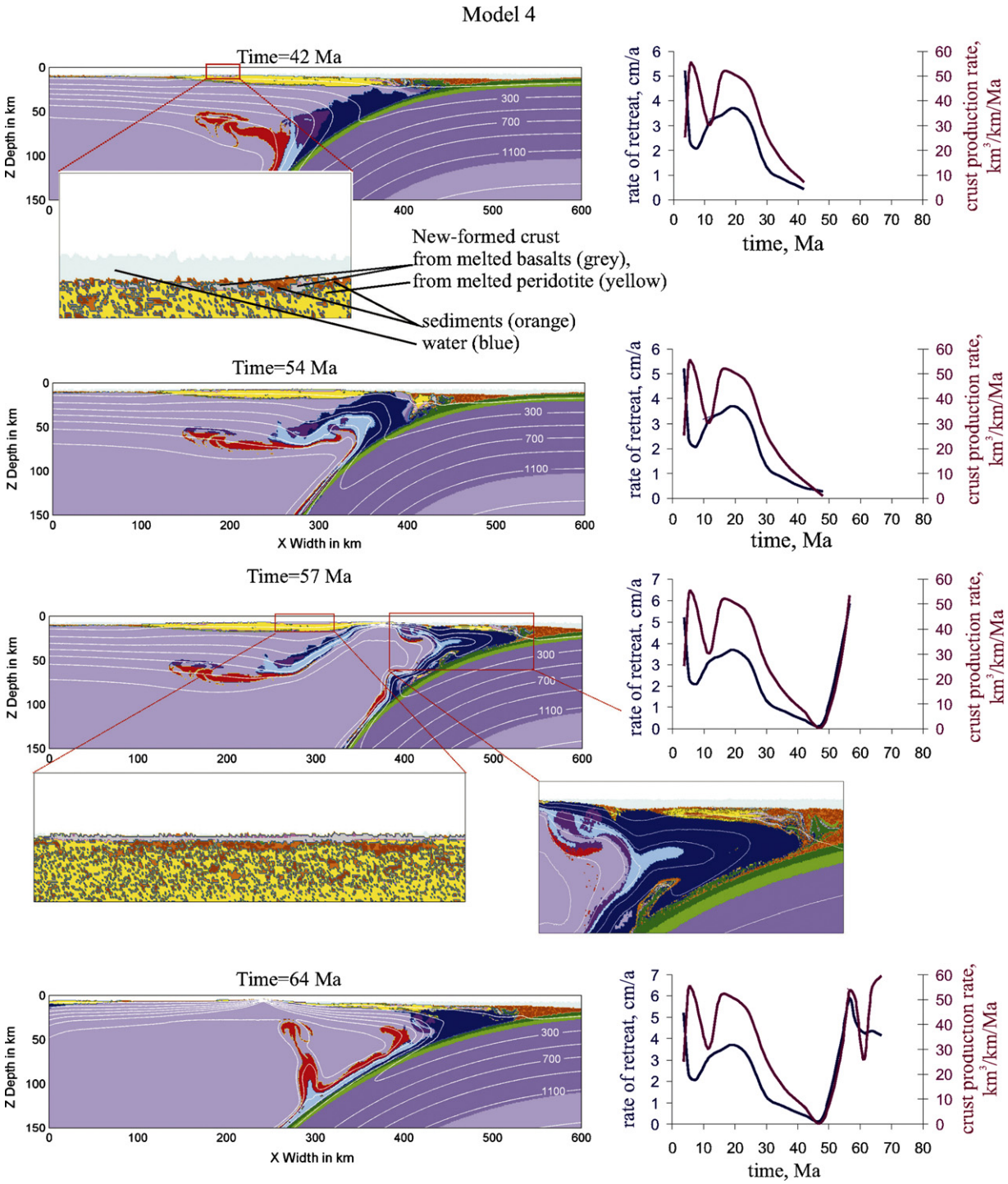

Fig. 7. Development of an extensional regime and opening of new spreading center following to the relatively slow rate of retreat and thermal relaxation of the slab. Left column: evolution of lithological field (color grid as on the Fig. 1); right column: rate of retreat as a function of time; in the insets: zoomed areas of new-formed crust structure and circulation of crust material induced within serpentinized mantle. See text for details.

subducting plate (Gorczyk et al., 2007c). Serpentinized channel is another way to convey depleted mantle rocks to the surface (Liu and Jin, 2006).

The subduction rate (which match trench retreat rate for our models with the fixed right plate) varies strongly with time. In all our models, this rate slow (from 4 to 7 cm/y to 1–2 cm/y) a few Ma after the beginning of subduction and then rises to 4 cm/y. Two scenarios can be distinguished: (1) decay and, ultimately, the cessation of subduction, (2) increase in subduction rate (up to 12 cm/y) and stabilization of subduction.

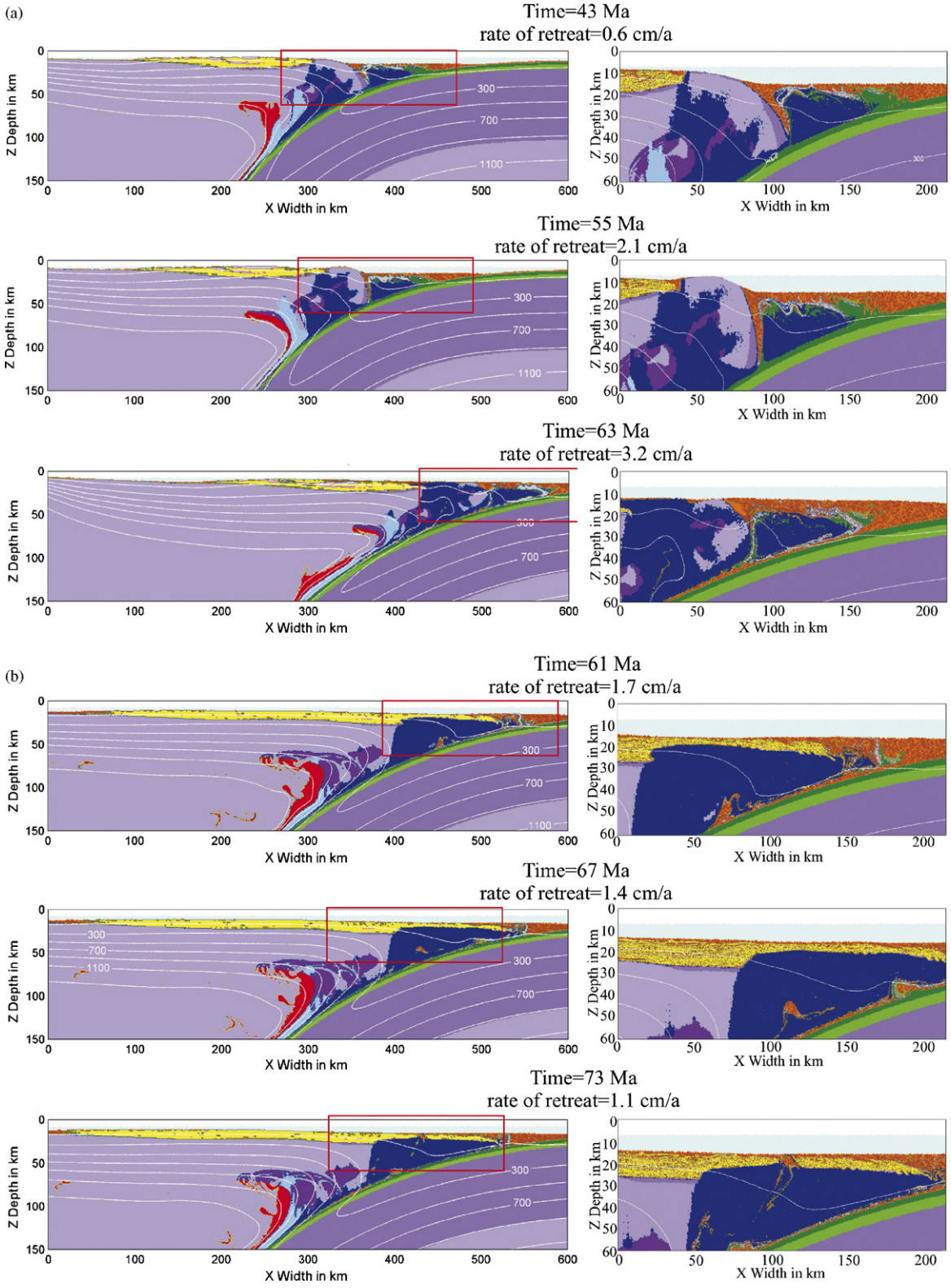

Fig. 8. Frames of two experiments with an entrainment of crust material into serpentinized channel. Types of source material: (a) subsurface material of the overriding plate (sediments and basalts from accretion prism) grabbed into the mantle (model 21, Table 4); (b) crustal material ascending from subducting slab (model 24, Table 4).

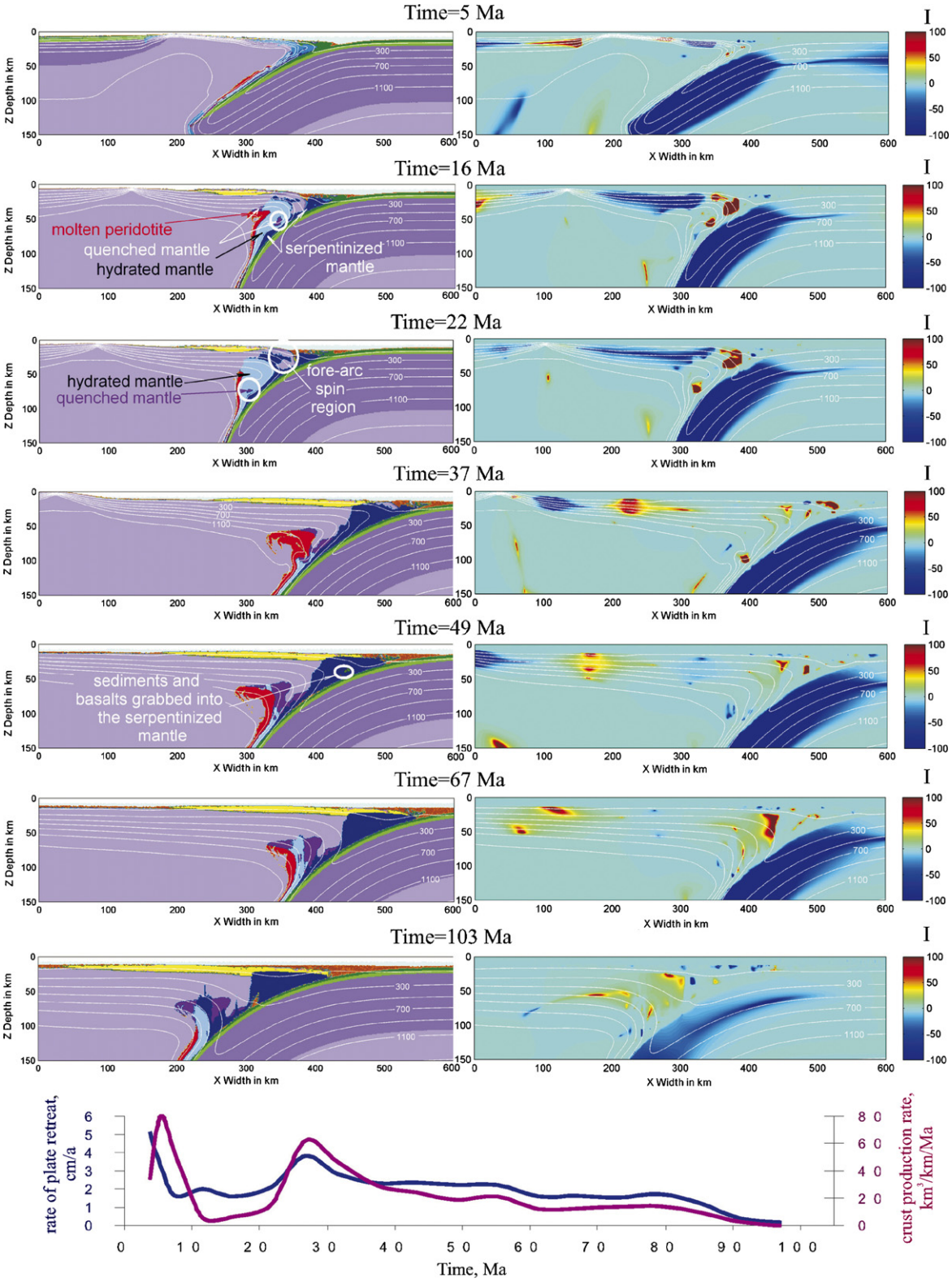

Fig. 9. Relative intensity of rotation (I) and its changes with time (right column) and corresponding evolution of lithological field (left column). $I = ((\partial v_z/\partial x)(\partial v_x/\partial z))/(2\dot{\varepsilon}_{II})$, where $\dot{\varepsilon}_{II}$ is the second invariant of strain rate tensor. Model 5, Table 4. Most prominent rigid body rotation features are: fore-arc spin (time = 22 Ma), subduction wheel (time = 16 Ma and 22 Ma), and wedge pin-balls (49 Ma). See text for details. Changes of rate of plate retreat and rate of crust production with time for this model is depicted below.

In several experiments subduction goes through both scenarios: it stops in after 10–50 My and then resumes later.

Several experiments in which subduction rate slows to ≤0.8 cm/y are characterized by thermal relaxation and partial melting of the slab. This phase is followed by re-initialization of subduction due to fore-arc extension and opening of new spreading center. The extension is triggered by the rheological weakening of the overriding plate, due to serpentinization in the fore-arc region, which leads to the splitting of previously formed crust thereby promoting subduction (Fig. 7).

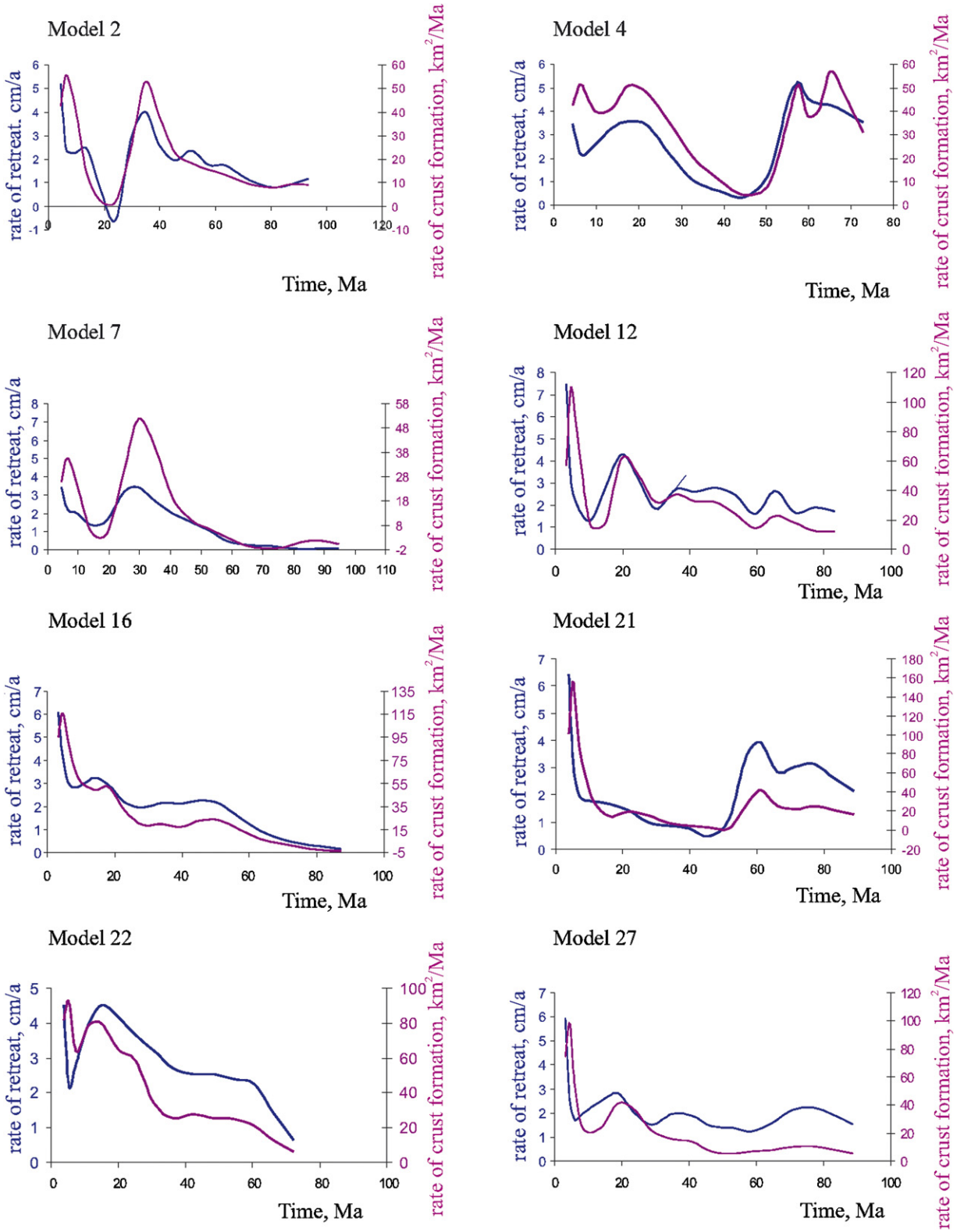

Fig. 10. Concordant changing with time of rate of plate retreat (cm/y) and rate of crust production (km^3/(km Ma)). See correlation coefficients for all experiments in Table 5.

The dynamics of subduction and magmatic arc growth depend strongly on the imposed rate of water transport (Table 4). A reduction in the rate of fluid expulsion leads to a narrowing of the hydration zone that, in turn, causes stronger plate coupling and lowers the rate of trench retreat. With only one exception (model 5′1) subduction ceases after 10–40 Myrs if the water transport speed is <0.09 m/y.

In agreement with previous studies that explored models with a kinematically prescribed subducting plate (Gerya et al., 2002, 2004a,b; Gorczyk et al., 2006) various types of serpentinized channel circulation (Fig. 8) and rigid body rotation (Fig. 9) phenomena occur in our numerical experiments. Prominent rigid body rotation features are observed close to the slab and are classified as (Gorczyk et al., 2006):

- Fore-arc spin: lithospheric part of the overriding plate bounded by new-formed oceanic crust, serpentinized mantle and slab (Fig. 9, 21.75 Ma).
- Subduction wheel: fragments of quenched strong dry mantle within hydrated mantle wedge found at asthenospheric depth (Fig. 9, 16.19 Ma). After crystallization of basalts the residue of peridotite becomes heavier and starts to sink, while new parts of buoyant hydrated mantle rocks are still arising. In several cases quenched rest of molten peridotite is separated into small pieces within hydrated mantle and begins to rotate during its continuous descending due to the moment between subducted slab and rising plume.
- Wedge pin-balls: rigid body rotation of crustal material entrained within the serpentinized channel (Fig. 9, 49.17 Ma). Entrainment of distinct fragments of the crust into the serpentinized channel can often be distinguished without quantity analysis of rotation. They circulate within serpentinized mantle (Figs. 7–9) and have two different sources: either this material ascends from the top of subducted plate with reverse flow (Figs. 7, 8b and 9) or it can be subsurface material (from a new crust or/and accretion prism) grabbed into the mantle (Fig. 8a). The second process usually takes place during temporary decay of subduction (when the rate of retreat for some period is less than 1 cm/y and then increases).

3.2. Dynamics of crust growth

Plume development and consequent arc growth rate correlate positively with rate of subduction/trench retreat (Fig. 10). This rate is calculated from the change in trench position with time. The locus of the trench is defined as the lowest point on the surface (Eq. (5)) between oceanic plate and water. Correlation coefficients between velocity of plate retreat and rate of accumulation of newly formed oceanic crust are listed in the Table 5. Their values are usually higher than 0.7. Low coefficients occur in cases of experiments when subduction intermittently ceases.

This dependence of rate of crust production on the subduction rate follows from the relationship between water release and hydrous mantle melting. Faster subduction increases the amount of water (i.e. of hydrated crustal rocks) subducted per unit time and therefore increases the amount of water released into the mantle wedge per unit time. The high rate of crust production does not necessarily result in large crustal volumes during experiment because the duration of the corresponding subduction may be short.

The volume of arc crust also depends on both the efficiency of melt extraction and the slab age (Fig. 11). With high melt extraction efficiency (M_{max} < 2%) the largest amount of crust is produced by oldest slabs (~3030 km^3/km crust after 2100 km of trench retreat,

Table 5
Correlation coefficient between rate of retreat of subducted plate and rate of accumulation of newly formed oceanic crust

Melt threshold	Age of subducted plate		
	40 Ma	70 Ma	100 Ma
0.2	0.88	0.59	0.83
0.4	0.78	0.64	0.69
1	0.94	0.88	0.87
2	0.78	0.91	0.58
4	0.76	0.8	0.91
6	0.39	0.9	0.74
10	0.92	0.85	0.54
14	0.76	0.87	0.56
18	0.87	0.7	0.78
30	0.7	0.67	0.46

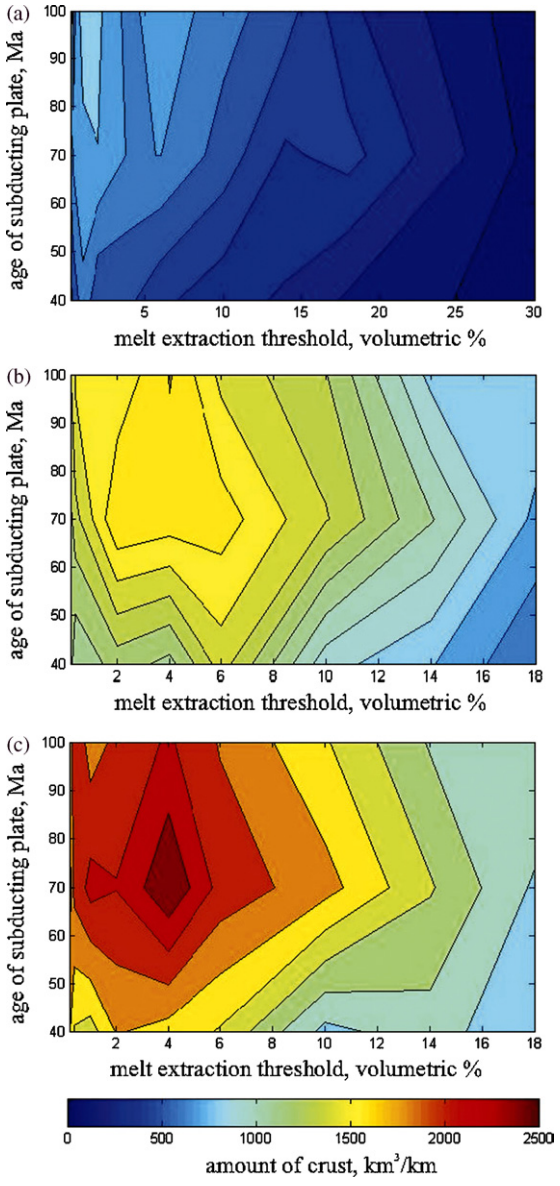

Fig. 11. Area diagrams representing crust production (volume per unit width along the strike direction of arc, km^3/km) as a function of both the slab age (40, 70, 100 Ma) and melt extraction intensity (melt extraction threshold varies from 0.2 to 30 vol.% of melt fraction – Table 4). (a) Volume of crust produced up to 500 km of trench retreat, (b) up to 1000 km of trench retreat, and (c) up to 1500 km. Note, that experiments with high melt extraction threshold are usually characterized by shorter duration of subduction. That is impressed at the pictures by absence of value at >18% threshold of melt extraction at 1000 km and1500 km of retreat (b and c).

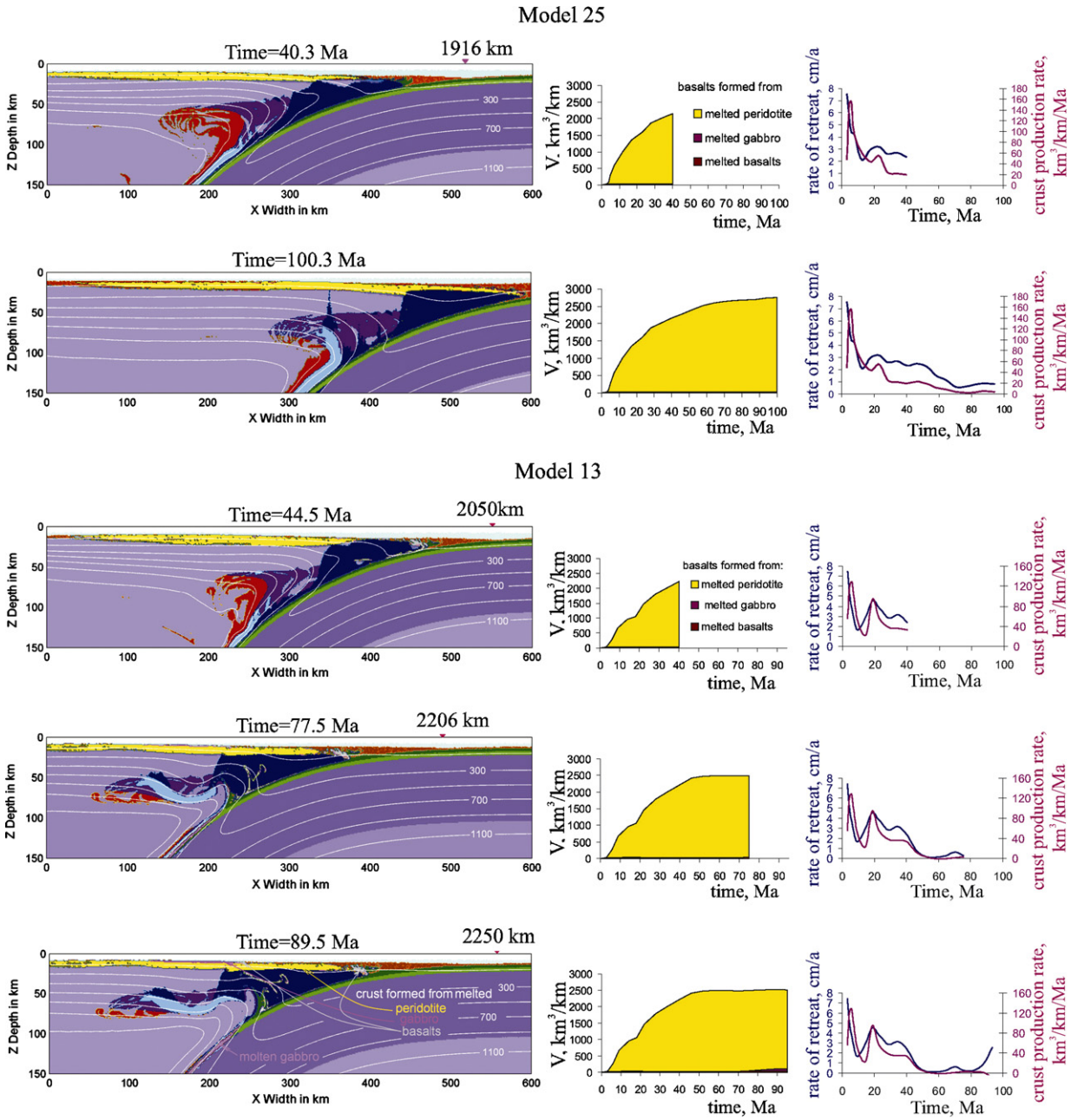

Fig. 12. Two different scenarios of subduction evolution and corresponding newly formed crust compositions. Left column: evolution of lithological field (color grid as on the Fig. 1); in the middle: evolution of amount (volume per unit width along the strike direction of arc) of different components building up magmatic arc as a function of time; right column: both rate of plate retreat and rate of crust production as a function of time. (a) Stable subduction and formation of basalts related to the mantle melting (model 25, Table 4); (b) cessation of subduction and producing of three different types of crust components (model 13, Table 4). See text for more details and Fig. 13 for zoomed pictures.

whereas younger slabs yield ~2700 km^3/km crust at the same conditions). Intermediate extraction efficiency (2% < M_{max} < 6%) and slab age (70 My) maximizes crustal growth (~3511 km^3/km crust after 2000 km of trench retreat). Low melt extraction efficiency (M_{max} > 6%) leads to low crustal generation for all slab ages.

3.3. Composition of newly formed crust

The arc crust is composed of rocks that may be derived by melting from the mantle or any of the three subducted crustal lithologies (sediments, basalts, gabbroic rocks). The mantle-derived component is always dominant. In all studied cases the mantle component appears shortly after beginning of subduction and remains present as long as subduction is active.

Small amounts of rocks related to subducted oceanic crust melting are also generated shortly after the beginning of subduction in all experiments (~16 km/km^3). This result is explained by melting of the leading edge of the slab (slab nose) due to the large thermal contrast with the mantle. This process is documented for young subduction zones (Sajona et al., 1993). A more significant slab component appears during later stage of subduction process when subduction rate slows causing the slab to heat up, but decreasing subduction rate also reduces the water influx to the mantle wedge responsible for promoting melting. Given these counter-

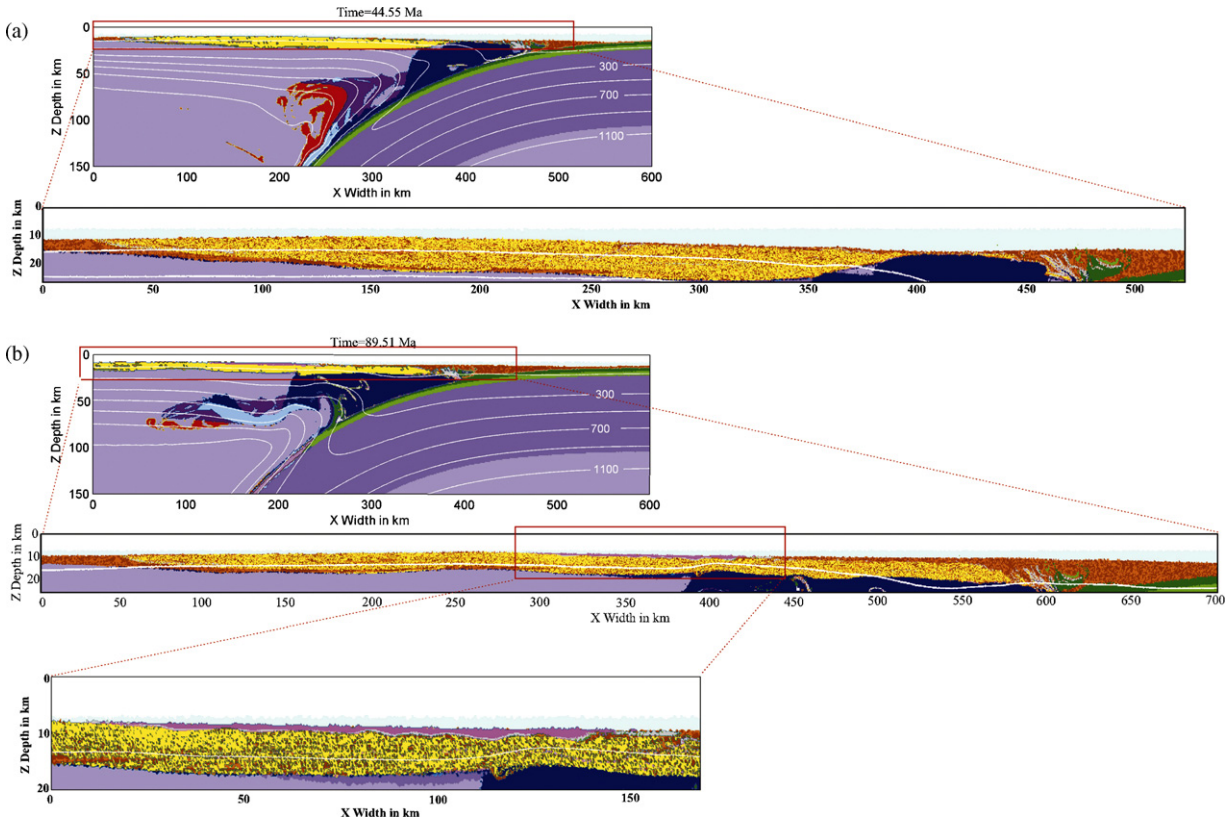

Fig. 13. Structure of new-formed crust. (a) In case of stable subduction (model 25, Table 4), (b) in case of cessation of subduction (model 13, Table 4). Color grid is as on the Fig. 1.

acting factors, a reduction of mantle component and appearance of slab constituent is to be expected with time. Under this conjecture the first rock type related to the subducted plate melting should be from melted sediments (the first layer in oceanic crust). However, the sedimentary component in our models is always insignificant, an effect that is explained by small sedimentary input. The basalt component first appears for subduction rates <0.9 cm/y (Figs. 7, 12 and 13), and the gabbro component appears only in case of cessation of subduction and always after the basaltic component (Figs. 12 and 13, Gerya et al., 2004b). These regularities are consistent with common assertions that rock in subducted ocean crust is too cold to melt at sub-arc depth in most modern active subduction zones (Peacock et al., 1994; Schmidt and Poli, 1998; Macpherson et al., 2006) and that subducted crustal rocks only undergo significant melting when they are entrained in hydrous diapiric upwellings rising from the slab into the hot portion of the mantle wedge (Gerya and Yuen, 2003b; Gerya et al., 2004a, 2006; Gorczyk et al., 2007a,b). Indeed, Kelemen et al. (2003) argue that temperature profile of subduction zones could allow partial melting of subducted material even for old slab and fast subduction which is in contrast to our models. This discrepancy is due primarily to model configuration, in that Kelemen et al. (2003) explored kinematically prescribed models of subduction with strain rate independent mantle viscosity.

4. Discussion

Synthetic seismic tomographic images generated from our models (Figs. 14 and 15) provide a basis for comparing the models with the observed tomographic structures in mantle wedges. Our model results suggest that within subducted oceanic crust seismic velocity anomalies change sign with depth due to dehydration. As also inferred from natural and experimental data (Bostock et al., 2002; Poli and Schmidt, 1995), the subducted model crust releases large amounts of fluid at shallow depth, hence at these depths (ca. <50 km) the velocity profile is highly variable. At greater depths, prominent negative anomalies are located in the gabbroic section of the subducted crust at depths 100–200 km reflecting the presence of hydrous minerals (e.g. lawsonite and phengite) as consistent with experimental phase equilibria data (e.g. Poli and Schmidt, 1995; Pawley and Holloway, 1993).

The seismic structure of the mantle wedge changes during subduction and plume propagation. The main structural features of our models are

1. A negative anomaly related to a serpentinite layer located immediately above the slab at both shallow and asthenosperic depths (100–150 km, Figs. 14 and 15). The presence of this layer is consistent with natural data (Iwamori, 1998; Bostock et al., 2002; Kawakatsu and Watada, 2007). For example, Kawakatsu and Watada (2007) found a negative velocity anomaly parallel to the slab beneath northeast Japan. They interpreted the anomaly as a boundary between overlying serpentinized low-velocity mantle layer and oceanic crust. At later stages of subduction (Fig. 15) this negative anomaly broadens in the fore-arc lithosphere. This broadening is due to growth of the serpentinized channel (e.g. Gerya et al., 2002). This feature is consistent with the seismic data from, e.g. the Cascadia subduction zone, where a negative anomaly of comparable extent and position is associated with an inverted Moho signature and attributed to the presence of

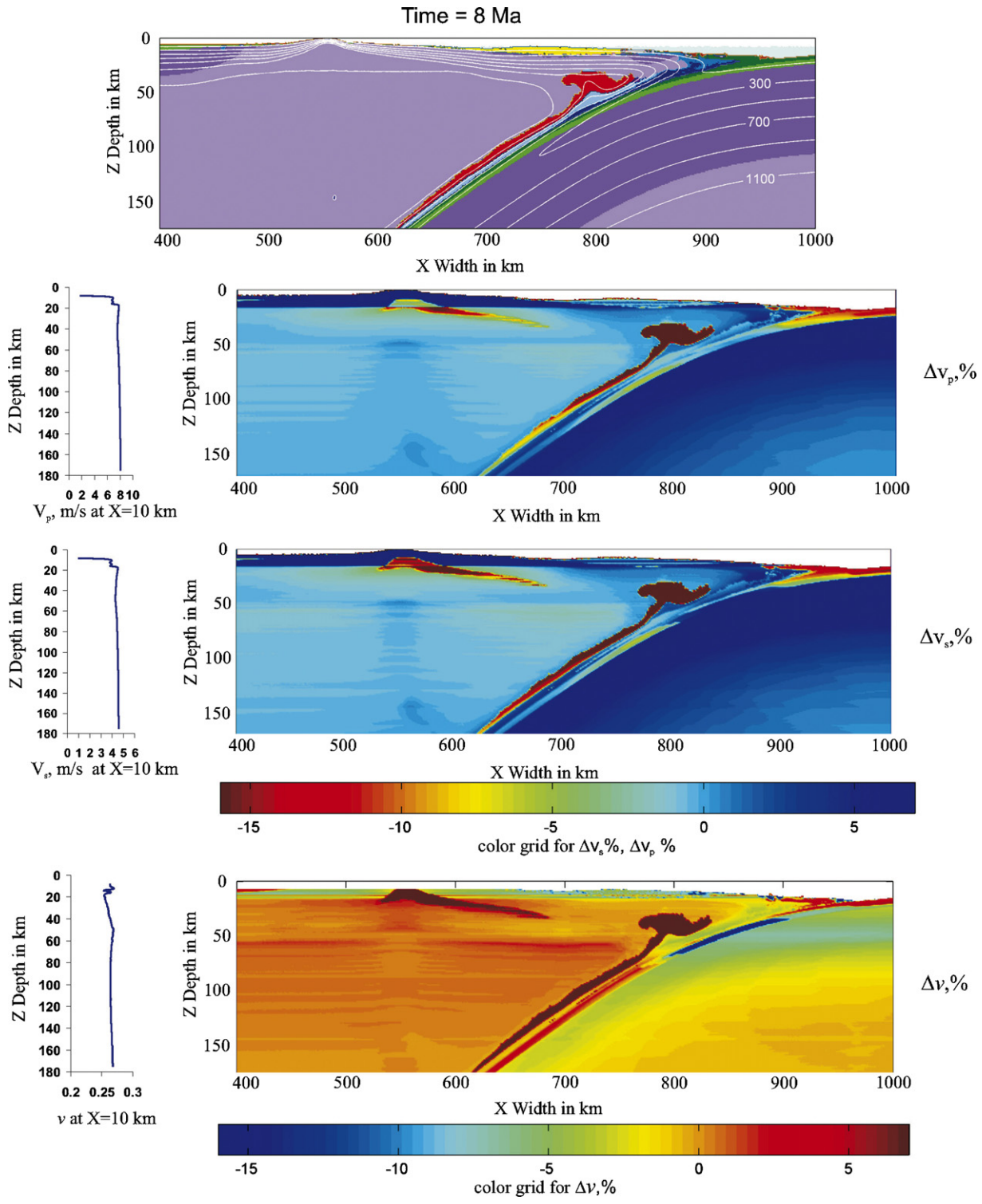

Fig. 14. Synthetic seismic tomographic images and corresponding lithological and temperature field (the upper picture). Model 25, Table 4, time = 7.63 Ma. Variations in v_p (compression wave seismic velocity), v_s (shear wave seismic velocity), and ν (Poisson's ratio) were computed relative to the vertical profile in the mantle at $x = 10$ km (see left column at the picture).

serpentinized peridotite in the overriding plate (Bostock et al., 2002).

2. Strong negative anomalies correspond to molten peridotite in the hot portion of the mantle wedge (Figs. 14 and 15).
3. Strong shallow negative anomalies reveal a back-arc spreading center, where hot mantle material raises toward the surface (Fig. 14).

Our models show (Figs. 14 and 15) strong positive Poisson's ratio anomalies for molten plumes in the mantle wedge (often >10%). At <70 km depth, Poisson's ratio of the model oceanic crust decreases as slab rocks undergo progressive metamorphism, thereafter the crustal Poisson's ratio increases (the deviation from standard profile changes from <−6% to >1%). These changes are consistent with the average Poisson's ratios of basalt (0.29), green-schist and

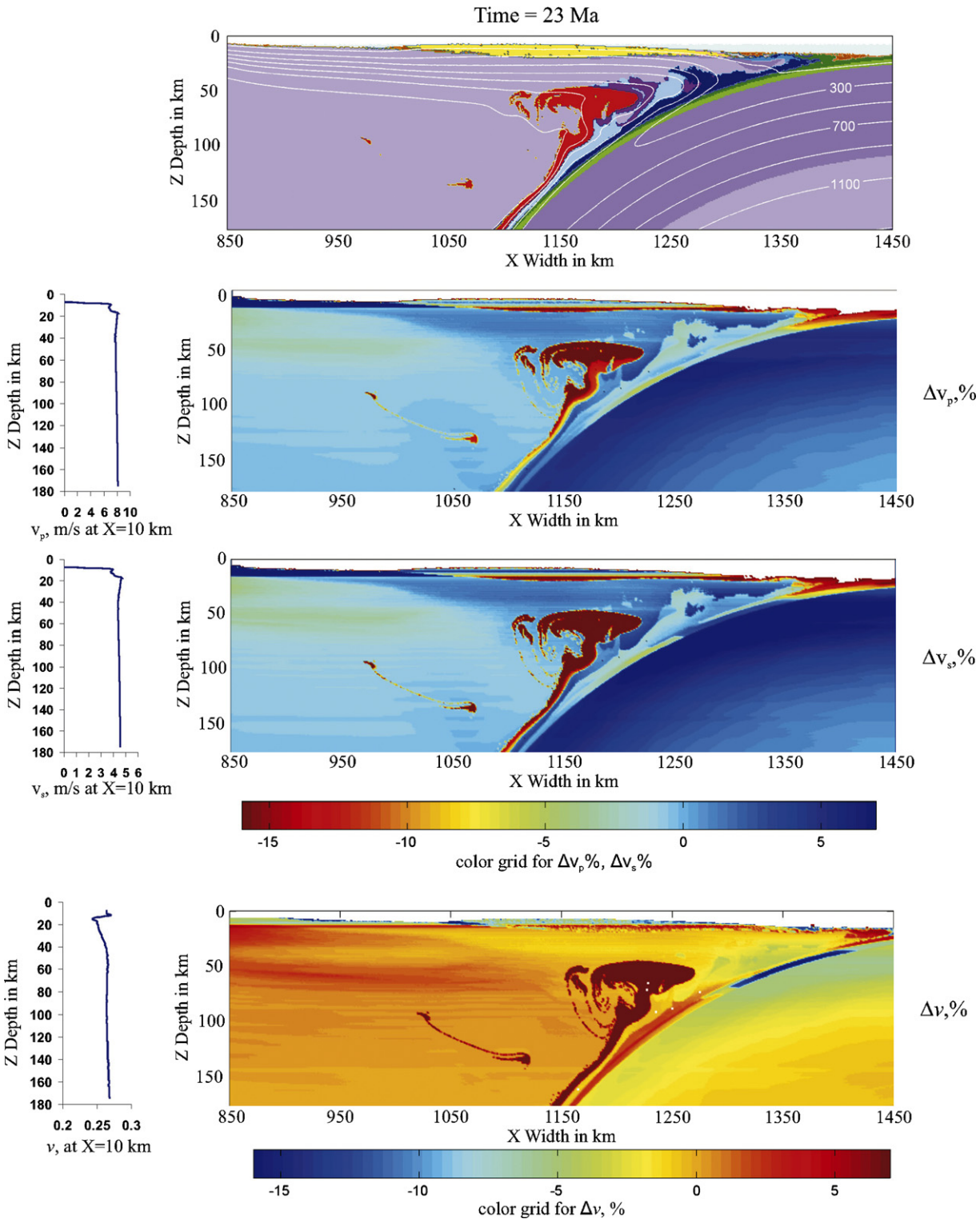

Fig. 15. Synthetic seismic tomographic images analogous to the images at Fig. 13, but representing later stage of subduction (time = 23.16 Ma, model 25, Table 4).

amphibolite facies rocks (0.26) and granulite facies rocks (0.28) as reported by Christensen (1996) as well as with calculated V_p/V_s ratios reported by Hacker et al. (2003).

Based on the total arc crust volume divided by the oldest known igneous age, Reymer and Schubert (1984) estimated rates of crustal generation as 20–40 km^3/(km Ma) for the western Pacific region. More recent estimates for the same area by Taira et al. (Izu-Bonin island arc, 1998), Holbrook et al. (Aleutian island arc, 1999) and Dimalanta et al. (Tonga, New Hebrides, Marianas, Southern and Northern Izu-Bonin, Aleutian island arcs, 2002) are somewhat higher, 40–95 km^3/(km Ma) and are much higher, 120–180 km^3/(km Ma), according to the work of Stern and Bloomer (early stage of IBM development, 1992). Our experiments show average rates of crust accumulation of 30–50 km^3/(km Ma)

Table 6
Average rate of plate retreat and corresponding crustal growth average rate

Model	Slab age (Ma)	Melt extraction threshold (vol.%)	Rate of plate retreat v (km/Ma)	Rate of crustal growth $\partial V/\partial t$ (km^3/(km Ma))
1	40	0.2	21.9	30.2
2	40	0.4	20.7	21.8
3	40	1	10.7	13
4	40	2	30.1	35.2
5	40	4	21.6	23.8
6	40	6	28.2	28.3
7	40	10	19.4	20.4
8	40	14	22.8	15.56
9	40	18	24.1	13.3
10	40	30	25.0	5
11	70	0.2	24.1	33
12	70	0.4	27.2	36.4
13	70	1	32.2	51.4
14	70	2	28.4	49.5
15	70	4	29.1	49.6
16	70	6	22.9	40.3
17	70	10	22.6	28.3
18	70	14	20.9	23.6
19	70	18	20.1	12.6
20	70	30	21.4	2.8
21	100	0.2	25	34
22	100	0.4	29.8	44.8
23	100	1	28.5	38.6
24	100	2	25.4	38
25	100	4	25.6	38.9
26	100	6	24.2	42.9
27	100	10	22.7	25.2
28	100	14	22.6	23.9
29	100	18	30.2	26
30	100	30	10	0.6

(Table 6). Thus, our values are close to the lower limit of the range for real arcs. This is explicable in view of three limitations of our model:

(1) The absence of dry mantle melting (e.g. Cooper et al., 2002). Stern and Bloomer (1992) showed that the early stage of IBM subduction was strongly extensional and decompression melting gave a substantial contribution to the magmatic activity. Tamura et al. (2005) suggested that degree of partial melting of a dry source mantle is ~10%, and degree of melting of hydrous source mantle is ~20% in the Simusu magmatic system, Izu-Bonin arc.
(2) The water content at the wet-solidus for mantle peridotite is assumed to be 2 wt.%. This value may be overestimated (Peacock, 1987; Davies, 1999), lower values would increase the volume of melt generated by the models. More realistic models of mantle wedge melting (e.g. Grove et al., 2006) might also improve accuracy of numerical results.
(3) Average rates of spontaneous subduction in our experiments (Table 6) are roughly half those estimated for real arcs. For example, the convergence rate across Tonga trench, where average rate of crust addition considered by Dimalanta with co-authors was 56 km^3/(km Ma) during last 27 Ma, varies from 16.5 cm/y in the south to 24 cm/y in the north (Pelletier et al., 1998; Bevis et al., 1995). In our numerical experiments, the rate of trench retreat is always <10 cm/y. Our experiments show that increasing in plate velocity would lead to significant increasing in rate of crustal growth.

5. Conclusions

We have examined the influence of melt extraction intensity, age of subducted plate, and velocity of water propagation on the dynamics of subduction and crust development. We conclude that:

1. There is a strong positive correlation between velocity of plate retreat and rate of crust accumulation.
2. Crust formed by mantle wedge melting is predominant in the magmatic arc. The contribution from melting of subducted crust is only significant (>60 km^3/km) after the cessation of subduction, which allows thermal relaxation of the slab.
3. The volume of new-formed crust is strongly correlated with the age of the subducted plate and the threshold for melt extraction. On a 10–100 Ma time-scale magmatic arc growth is maximized by a slab of intermediate age (70–100 Ma) with an intermediate melt extraction threshold (2–6%).

Acknowledgements

This work was supported by ETH Research Grant TH-12/05-3 and SNF Research Grant 200021-113672/1. B. Burdon is thanked for fruitful discussions. Constructive suggestions by two anonymous reviewers are greatly appreciated.

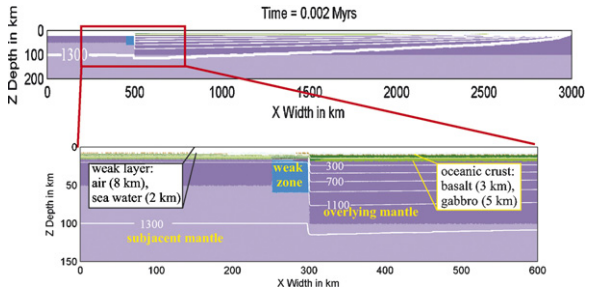

Fig. A1. Initial configuration of an additional numerical experiment (model 5-ad). It replicates setup of the model 5 except the age (temperature profile) of subducting plate. The age of an older plate diminishes away from the initial weak zone between plates to 1 year at the right end of the plate.

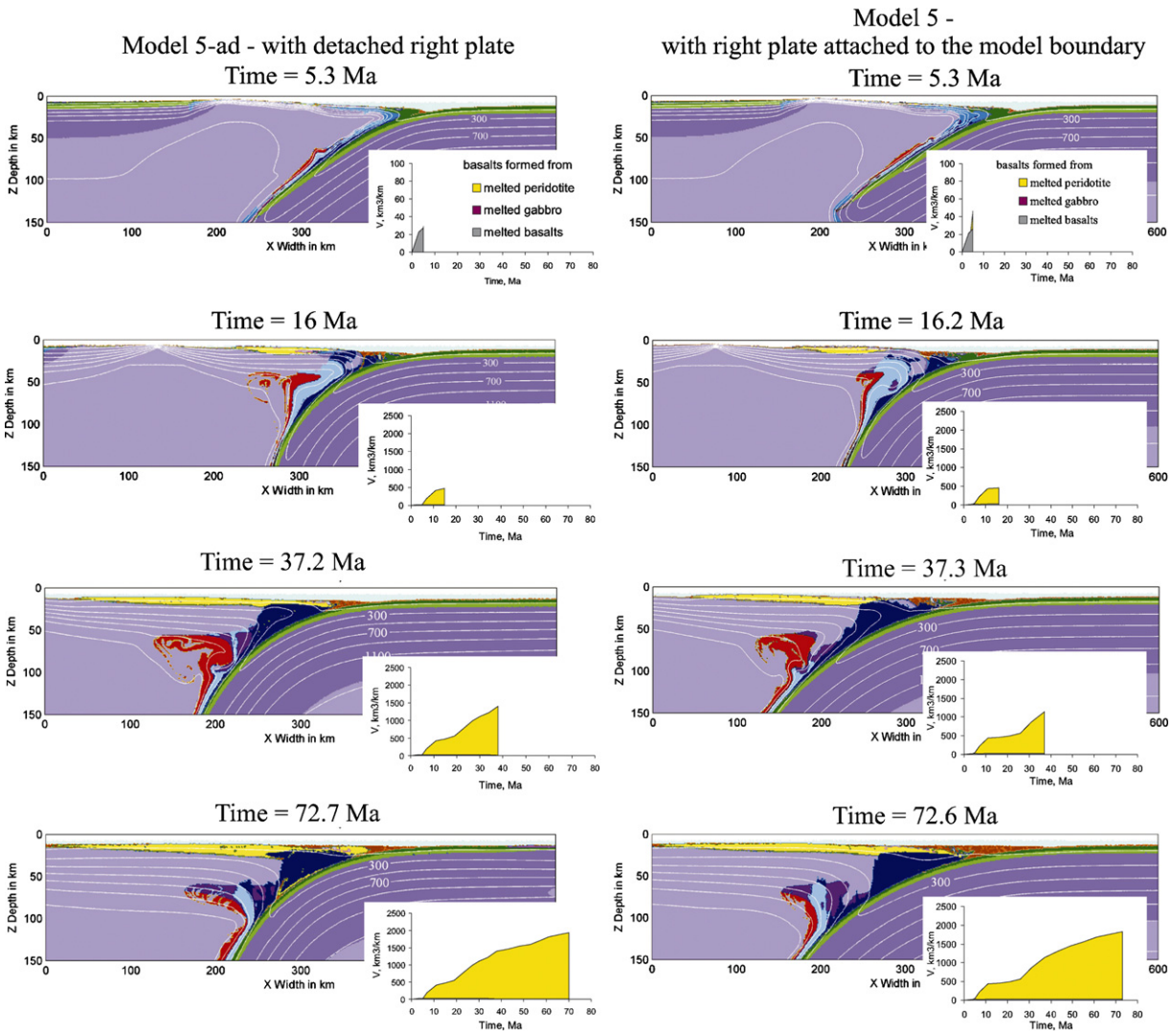

Fig. A2. Frames of two experiments: model 5 with attached subducting plate to the right boundary (right column), and model 5-ad, where plate is detached from the right boundary (left column). See text for the details.

Appendix A. Influence of the detached subducting plate

Subducted plate in our model is attached to the right boundary, thus subduction is manifest by the retreat of the subducted plate. To check sensitivity of our results to this model feature we ran an experiment where the subducting plate was detached from the right model boundary (Fig. A1). As a reference model we chose model 5, with an intermediate melt extraction threshold and slab age of 40 Ma. The results (model 5-ad) show no important differences in development or crustal production (Fig. A2). The most evident difference being the angle of slab subduction, which is steeper in a model 5-ad.

References

Armstrong, R.L., 1971. Isotopic and chemical constraints on modelis of magma genesis in volcanic arcs. Earth and Planetary Science Letters 12, 137–142.

Behn, M.D., Kelemen, P.B., 2003. Relationship between seismic P-wave velocity and the composition of anhydrous igneous and meta-igneous rocks. Geochemistry Geophysics Geosystems 4, doi:10.1029/2002GC000393.

Bevis, M., Taylor, F.W., Schutz, B.E., Recy, J., Isacks, B.L., Helu, S., Singh, R., Kendrick, E., Stowell, J., Taylor, B., Calmant, S., 1995. Geodetic observations of very rapid convergence and back-arc extension at the Tonga arc. Letters to Nature 374, 249–251.

Bostock, M.G., Hyndman, R.D., Rondenay, S., Peacock, S.M., 2002. An inverted continental Moho and serpentinization of the forearc mantle. Nature 417, 536–538.

Carlson, R.L., 2001. The abundance of ultramafic rocks in Atlantic Ocean crust. Geophysical Journal International 144, 37–48.

Carlson, R.L., Miller, D.J., 2003. Mantle wedge water contents estimated from seismic velocities in partially serpentinized peridotites. Geophysical Research Letters 30 (5).

Christensen, N.I., 1996. Poisson's ration and crustal seismology. Journal of Geophysical Research 101, 3139–3156.

Clauser, C., Huenges, E., 1995. Thermal conductivity of rocks and minerals. In: Ahrens (Ed.), Rock physics and phase relations - a handbook of physical constrants, AGU Reference Shelf. American Geophysical Union, pp. 105–126.

Connolly, J.A.D., 2005. Computation of phase equilibria by linear programming: a tool for geodynamic modeling and its application to subduction zone decarbonation. Earth and Planetary Science Letters 236, 524–541.

Connolly, J.A.D., Kerrick, D.M., 2002. Metamorpic controls on seismic velocity of subducted oceanic crust at 100–250 km depth. Earth and Planetary Science Letters 204, 61–74.

Connolly, J.A.D., Petrini, K., 2002. An automated strategy for calculation of phase diagram sections and retrieval of rock properties as a function of physical conditions. Journal of Metamorphic Geology 20, 697–708.

Cooper, K.M., Reid, M.R., Dunbar, N.W., McIntosh, W.C., 2002. Origin of mafic magmas beneath northwestern Tibet: constraints from ^{230}Th–^{238}U disequilibria. Geochemistry Geophysics Geosystems 3 (11), doi:10.1029/2002GC00032.

Davies, J.H., 1999. The role of hydraulic fractures in generating intermediate depth earthquakes and subduction zone magmatism. Nature 398, 142–145.

Davies, J.H., Stevenson, D.J., 1992. Physical model of source region of subduction zone volcanics. Journal of Geophysical Research – Solid Earth 97, 2037–2070.

Dimalanta, C., Taira, A., Yumul Jr., G.P., Tokuyama, H., Mochizuki, K., 2002. New rates of western Pacific island arc magmatism from seismic and gravity data. Earth and Planetary Science Letters 202, 105–115.
Elburg, M.A., van Bergen, M.J., Foden, J.D., 2004. Subducted upper and lower continental crust contributes to magmatism in the collision sector of the Sunda-Banda arc, Indonesia. Geology 32, 41–44.
Elliott, T., Plank, T., Zindler, A., Wjite, W., Bourdon, B., 1997. Element transport from slab to volcanic front at the Mariana arc. Journal of Geophysical Research 102, 14991–15019.
Encarnacion, J., 2004. Multiple ophiolite generation preserved in the northern Philippines and the growth of an island arc complex. Tectonophysics 392, 103–130.
George, R., Turner, S., Hawkesworth, C., Morris, J., Nye, C., Ryan, J., Zheng, S.-H., 2003. Melting processes and fluid and sediment transport rates along the Alaska–Aleutian arc from an integrated U–Th-Ra-Be isotope study. Journal of Geophysical Research 108, doi:10.1029/2002JB001916.
Gerya, T.V., Burg, J.P., 2007. Intrusion of ultramafic magmatic bodies into the continental crust: numerical simulation. Physics of the Earth and Planetary Interiors 160, 124–142.
Gerya, T.V., Connolly, A.D., Yuen, D.A., Gorczyk, W., Capel, A.M., 2006. Seismic implications of mantle wedge plumes. Physics of the Earth and Planetary Interiors 156, 59–74.
Gerya, T.V., Stöckhert, B., Perchuk, A.L., 2002. Exhumation of high-pressure metamorphic rocks in a subduction channel: a numerical simulation. Tectonics 21 (6), 6-1–6-19.
Gerya, T.V., Yuen, D.A., 2003a. Characteristics-based marker-in-cell method with conservative finite-differences schemes for modeling geological flows with strongly variable transport properties. Physics of the Earth and Planetary Interiors 140, 293–318.
Gerya, T.V., Yuen, D.A., 2003b. Rayleigh-Taylor instabilities from hydration and melting propel 'cold plumes' at subduction zones. Earth and Planetary Science Letters 212, 47–62.
Gerya, T.V., Yuen, D.A., Sevre, E.O.D., 2004a. Dynamical causes for incipient magma chambers above slabs. Geology 32, 89–92.
Gerya, T.V., Yuen, D.A., Maresch, W.V., 2004b. Thermomechanical modeling of slab detachment. Earth and Planetary Science Letters 226, 101–116.
Gerya, T.V., Connolly, J.A.D., Yuen, D.A., 2008. Why is terrestrial subduction one-sided? Geology 36 (1), 43–46.
Ghiorso, M.S., Hirschmann, M.M., Reiners, P.W., Kress, V.C., 2002. The pMELTS: A revision of MELTS for improved calculation of phase relations and major element partitioning related to partial melting of the mantle to 3 GPa. Geochemistry Geophysics Geosystems 3, doi:10.1029/2001GC000217.
Gordienko, I.V., Filimonov, A.V., Minina, O.R., Gornova, M.A., Medvedev, A.Ya., Klimul, V.S., Elbaev, A.L., Tomurtogoo, O., 2007. Dzhida island-arc system in the Paleoasian Ocean: structure and main stages of Vendian–Paleozoic geodynamic evolution. Russian Geology and Geophysics 8, 91–106.
Gorczyk, W., Gerya, T.V., Connolly, J.A.D., Yuen, D.A., Rudolph, M., 2006. Large-scale rigid-body rotation in the mantle wedge and its implications for seismic tomography. Geochemistry Geophysics Geosystems 7, doi:10.1029/2005GC001075.
Gorczyk, W., Gerya, T.V., Connolly, J.A.D., Yuen, D.A., 2007a. Growth and mixing dynamics of mantle wedge plumes. Geology 35, 587–590.
Gorczyk, W., Willner, A.P., Connolly, J.A.D., Burg, J.-P., 2007b. Physical controls of magmatic productivity at Pacific-type convergent margins: new insights from numerical modeling. Physics of the Earth and Planetary Interiors 163, 209–232.
Gorczyk, W., Guillot, S., Gerya, T.V., Hattori, K., 2007c. Asthenospheric upwelling, oceanic slab retreat and exhumation of UHP mantle rocks: insights from Greater Antilles. Geophysical Research Letters 34 (21), doi:10.1029/2007GL031059 (article no. L21309).
Grove, T.L., Chatterjee, N., Parman, S.W., Médard, E., 2006. The influence of H_2O on mantle wedge melting. Earth and Planetary Science Letters 249, 74–89.
Hacker, B.R., Abers, G.A., Peacock, S.M., 2003. Subduction factory. 1. Theoretical mineralogy, densities, seismic wave speeds, and H_2O contents. Journal of Geophysical Research 108 (B1), doi:10.1029/2001JB001127.
Hall, C.E., Gurnis, M., Sdrolias, M., Lavier, L.L., Müller, R.D., 2003. Catastrophic initiation of subduction following forced convergence across fracture zones. Earth and Planetary Science Letters 212, 15–30.
Hassani, R., Jongmans, D., Chery, J., 1997. Study of plate deformation and stress in subduction processes using two-dimensional numerical models. Journal of Geophysical Research 102, 17,951–17,965.
Hawkesworth, C.J., Turner, S.P., McDermott, F., Peate, D.W., vanCalsteren, P., 1997. U–Th isotopes in arc magmas: implications for element transfer from the subducted crust. Science 276, 551–555.
Holbrook, W.S., Lizarralde, D., McGeary, S., Bangs, N., Diebold, J., 1999. Structure and composition of Aleutian island arc and implications for continental crustal growth. Geology 27, 31–34.
Holland, T., Backer, J., Powell, R., 1998. Mixing properties and activity–composition relationships of chlorites in the system MgO-FeO-Al_2O_3-SiO_2-H_2O. European Journal of Mineralogy 10, 395–406.
Holland, T., Powell, R., 1996. Thermodynamics of order - disorder in minerals. 2. Symmetric formalism applied to solid solutions. American Mineralogist 81, 1425–1437.
Holland, T.J.B., Powell, R., 1998. An internally consistent thermodynamic data set for phases of petrological interest. Journal of Metamorphic Geology 16, 309–343.
Iwamori, H., 1998. Transportation of H_2O and melting in subduction zones. Earth and Planetary Science Letters 160, 65–80.
Kawakatsu, H., Watada, S., 2007. Seismic evidence for deep-water transportation in the mantle. Science 316, 1468–1471.
Kelemen, P.B., Rilling, J.L., Parmentier, E.M., Mehl, L., Hacker, B.R., 2003. Thermal structure due to solid-state flow in the mantle wedge beneath arcs. AGU Monograph 138, 293–311.
Kelemen, P.B., Johnson, K.T.M., Kinzler, R.J., Irving, A.J., 1990. High-field-strength element depletions in arc basalts due to mantle-magma interaction. Nature 345, 521–524.
Kessel, R., Schmidt, M.W., Ulmer, P., Pettke, T., 2005. Trace element signature of subduction-zone fluids, melts and supercritical liquids at 120–180 km depth. Nature 437, 724–727.
Liu, X.W., Jin, Z.M., 2006. Microstructural features of ultrahigh-pressure garnet-peridotite from the Donghai district in the Sulu terrane: new evidence of rapid exhumation. Acta Petrologica Sinica 22 (7), 1810–1816.
Macpherson, C.G., Dreher, S.T., Thirlwall, M.F., 2006. Adakites without slab melting: high pressure differentiation of island arc magma, Mindanao, the Philippines. Earth and Planetary Science Letters 243, 581–593.
Melcher, F., Meisel, T., Puhl, J., Koller, F., 2002. Petrogenesis and geotectonic setting of ultramafic rocks in the Eastern Alps: constraints from geochemistry. Lithos 65, 69–112.
Morris, J.D., Hart, S.R., 1986. Isotopic and incompatible element constraints on the genesis of island-arc volcanics from Cold Bay and Amak island, Aleutians, and implications for mantle structure–Reply. Geochimica et cosmochimica acta 50, 483–487.
Newton, R.C., Charlu, T.V., Kleppa, O.J., 1980. Thermochemistry of the high structural state plagioclases. Geochemica et cosmochimica acta 44, 933–941.
Nimz, G.J., Cameron, K.L., Niemeyer, S., 1995. Formation of mantle lithosphere beneath northern Mexico: chemical and Sr–Nd–Pb isotopic systematics of peridotite xenoliths from La Olivina. Journal of Geophysical Research 100 (B3), 4181–4196.
Pawley, A.R., Holloway, J.R., 1993. Water sources for subduction zone volcanism: new experimental constraints. Science 260, 664–667.
Peacock, S.M., 1987. Serpentinization and infiltration metasomatism in the Trinity peridotite, Klamath province, northern California: implications for subduction zones. Contributions to Mineralogy and Petrology 95, 55–70.
Peacock, S.M., Rushmer, T., Thompson, A.B., 1994. Partial melting of subducting oceanic crust. Earth and Planetary Science Letters 121, 227–244.
Pelletier, B., Calmant, S., Pillet, R., 1998. Current tectonics of the Tonga-New Hebrides region. Earth and Planetary Science Letters 164, 263–276.
Plank, T., Langmuir, C.H., 1998. The chemical composition of subducting sediment and its consequences for the crust and mantle. Chemical Geology 145, 325–394.
Poli, S., Schmidt, M.W., 1995. H_2O transport and release in subduction zones: experimental constraints on basaltic and andesitic systems. Journal of Geophysical Research 100, 22299–22314.
Poli, S., Schmidt, M.W., 2002. Petrology of subducted slabs. Annual Review of Earth and Planetary Sciences 30, 207–235.
Powell, R., Holland, T., 1999. Relating formulations of the thermodynamics of mineral solid solutions: Activity modeling of pyroxenes, amphiboles, and micas. American mineralogist 84, 1–4.
Rannalli, G., 1995. Rheology of the Earth. Chapman and Hall, London, p. 413.
Regenauer-Lieb, K., Yuen, D., Branlund, J., 2001. The initiation of subduction: criticality by addition of water? Science 294, 578–580.
Reymer, A., Schubert, G., 1984. Phanerozoic addition rates to the continental crust and crustal growth. Tectonics 3, 63–77.
Rosner, M., Erzinger, J., Franz, G., Trumbull, R.B., 2003. Slab-derived boron isotope signatures in arc volcanic rocks from the Central Andes and evidence for boron isotope fractionation during progressive slab dehydration. Geochemistry Geophysics Geosystems 4 (8), doi:10.1029/2002GC000438.
Rupke, L.H., Morgan, J.P., Hort, M., Connolly, J.A.D., 2004. Serpentine and the subduction zone water cycle. Earth and Planetary Science Letters 223, 17–34.
Saal, A.E., Hart, S.R., Shimizu, N., Hauri, E.H., Layne, C.D., Eiler, J.M., 2005. Pb isotopic variability in melt inclusions from the EMI-EMII-HIMU mantle end-members and the role of the oceanic lithosphere. Earth and Planetary Science Letters 240, 605–620.
Sajona, F.G., Maury, R.C., Bellon, H., Cotton, J., Defant, M.J., Pubellier, M., 1993. Initiation of subduction and the generation of slab melts in western and eastern Mindanao, Philippines. Geology 21, 1007–1010.
Schmidt, M.W., Poli, S., 1998. Experimentally based water budgets for dehydrating slabs and consequences for arc magma generation. Earth and Planetary Science Letters 163, 361–379.
Sobolev, S.V., Babeyko, A.Y., 2005. What drives orogeny in the Andes? Geology 33, 617–620.
Staudigel, H., Hart, S., Schmincke, H., Smith, B., 1989. Cretaceous ocean crust at DSDP sites 417-418: carbon uptake from weathering versus loss by magmatic outgassing. Geochimica et cosmochimica acta 53, 3091–3094.
Stern, R.J., 2002. Subduction zones. Reviews of Geophysics 40.
Stern, R.J., Bloomer, 1992. Subduction zone infancy: examples from the Eocene Izu-Bonin-Mariana and Jurassic California arcs. Geological Society of America Bulletin 104, 1621–1636.
Stern, R.J., Kohut, E., Bloomer, S.H., Leybourne, M., Fouch, M., Vervoort, J., 2006. Subduction factory processes beneath the Guguan cross-chain, Mariana Arc: no role for sediments, are serpentinites important? Contributions to Mineralogy and Petrology 151 (2), 202–221.

Straub, S.M., 2003. The evolution of the Izu Boin-Mariana volcanic arcs (NW Pacific) in terms of major element chemistry. Geochemistry Geophysics Geosystems 4 (2), doi:10.1029/2002GC000357.

Tagawa, M., Nakakuki, T., Kameyama, M., Tajima, F., 2007. The role of history-dependent rheology in plate boundary lubrication for generating one-sided subduction. Pure and Applied Geophysics 164, 879–907.

Taira, A., Saito, S., Aoike, K., Morita, S., Tokuyama, H., Suyehiro, K., Takahashi, N., Shinohara, M., Kiyokawa, S., Naka, J., Klaus, A., 1998. Nature and growth rate of the Northern Izu-Bonin (Ogasawara) arc crust and their implications for continental crust formation. The Island Arc 7, 395–407.

Tamura, Y., Tani, K., Ishizuka, O., Chang, Q., Shukuno, H., Fiske, R.S., 2005. Are arc basalts dry, wet, or both? Evidence from the Sumisu Caldera Volcano, Izu-Bonin arc. Japanese Journal of Petrology 46 (9), 1769–1803.

Takahashi, E., Kushiro, I., 1983. Melting of a dry peridotite at high-pressures and basalt magma genesis. American Mineralogist 68, 859–879.

Tatsumi, Y., Hamilton, D.L., Nesbitt, R.W., 1986. Chemical characteristics of fluid phase from a subducted lithosphere and origin of arc magmas: evidence from high-pressure experiments and natural rocks. Journal of Volcanology and Geothermal Research 29, 293–309.

Tera, F., Brown, L., Morris, J., Sacks, I.S., 1986. Sediment incorporation in island-arc magmas: inferences from ^{10}Be. Geochimica et Cosmochimica Acta 50, 535–550.

Thompson, J.B., Hovis, G.L., 1979. Entropy of mixing of sanidine. American mineralogist 64, 57–65.

Turcotte, D.L., Schubert, G., 2002. Geodynamics. Cambridge University Press, p. 456.

Wei, C.J., Powell, R., 2003. Phase relations in high-pressure metapelites in the system KFMASH (K_2O-FeO-MgO-Al_2O_3-SiO_2-H_2O) with application to natural rocks. Contributions to Mineralogy and Petrology 145, 301–315.

White, R.W., Powell, R., Phillips, G.N., 2003. A mineral equilibria study of the hydrothermal alteration in mafic greenschist facies rocks at Kalgoorlie, Western Australia. Journal of Metamorphic Geology 21, 455–468.